

CERN-TH/99-123
 NTUA-73/99
 OUTP-98-89P
 hep-ph/9905272

On magnetic catalysis in even-flavor QED_3

K. Farakos, G. Koutsoumbas

*Department of Physics, National Technical University of Athens,
 Zografou Campus, 157 80 Athens, GREECE*

N.E. Mavromatos

*CERN, Theory Division, Geneva 23 CH-1211, Switzerland,
 and Dept. of Physics, Theoretical Physics, Univ. of Oxford, 1 Keble Rd., OX1 3NP, U.K.*

Arshad Momen

*Dept. of Physics, Theoretical Physics, Univ. of Oxford,
 1 Keble Rd., OX1 3NP, U.K.*

Abstract

In this paper, we discuss the role of an external magnetic field on the dynamically generated fermion mass in even-flavor QED in three space-time dimensions. We show that for weak fields this mass increases quadratically with increasing field, while at strong fields one crosses over to a mass scaling logarithmically with the external field. We also confirm this type of scaling behavior through quenched lattice calculations using the non-compact version for the gauge field. Both the zero and finite temperature cases are examined. A preliminary study of the fermion condensate in the presence of magnetic flux tubes on the lattice is also included.

I. INTRODUCTION

The particle mass generation via dynamical symmetry breaking has been a much-studied scenario in particle physics as well as in condensed-matter systems. In the recent years this phenomenon has been studied in the presence of background fields, such as constant external magnetic fields [1]- [9], following and extending the formalism developed by Schwinger [10]. The formalism has been applied to models that had gauge and/or four-fermion interactions.

It was found that such constant background configurations can enhance the dynamical symmetry breaking by driving the critical coupling to a smaller value and thus catalyzing the symmetry breaking. A concrete example of this phenomenon, of relevance to us in this work, is the dynamical chiral symmetry breaking of chiral symmetry in massless QED (in three and four dimensions) in the presence of an external magnetic field [1,2,6–8] where the dynamically generated fermion mass depends on the value of the external field.

In the context of effective field theories a physical understanding of the above-mentioned phenomenon can be presented as below. For strong magnetic fields the energy gap between the Landau levels (LLs) becomes very large and hence the effective fermionic degrees of freedom are the ones in the lowest Landau levels (LLLs). A low-energy effective action involving these LLL fermions can then be found by *integrating out* the higher Landau levels [5]. This action for QED_4 apart from the usual minimal coupling terms [5] also contains four-fermi interactions. The presence of these extra interactions is responsible for the appearance of a non-vanishing condensate for the LLL fermions. Although by naive power counting such four-fermi operators appear irrelevant (in the renormalization-group sense), it turns out that the anomalous dimensions of these operators depend on the magnitude of the external magnetic field [5]. Above a critical value of the external magnetic field they become relevant operators [4] and generate the chiral symmetry breaking. The situation is reminiscent of the case of three-dimensional multiflavor four-fermi theories, where naive power counting arguments contradict the relevance of the interactions, which can be established only after a large- N analysis [11].

The magnetically catalyzed mass generation in (2+1) dimensional QED may have interesting condensed-matter applications [7,8], given the suggestions that high-temperature superconductors can be described effectively by field theories like QED_3 [12] or by non-Abelian gauge models based on the group $SU(2) \times U(1)$ [13,7]¹. Indeed, there is experimental evidence for the opening of a second (superconducting) gap at the nodes of the gap in certain d-wave superconductors in the presence of strong external magnetic fields [14]. As remarked in [15], in the context of condensed-matter-inspired models, the scaling of the thermal conductivity with the external field is different between the gauge [7,8] and four-fermion theories [16]. Thus, a detailed study of the magnetically-induced chiral symmetry breaking phenomenon in the context of QED_3 is phenomenologically desirable, given that such studies may lead to more detailed experiments in the spirit of [14], that can probe deep in the structure of the novel high-temperature superconductors.

In (2+1) dimensions chiral symmetry can be defined only if the number of fermion flavors is even [17]. This fact is relevant for a planar high- T_c superconducting antiferromagnetic system [12,18] which comprises of two sublattices. Within a generalized [13] spin-charge separation framework [19], there will be two species of charged fermion excitations (called holons), one associated with each sublattice [12,13]. Finally, the (2+1) dimensional theory with even number of fermion flavors [7] can be viewed as a dimensional reduction of the four-dimensional effective Lagrangian of [5].

¹The relativistic (Dirac) nature of the fermion fields is justified by the fact that they describe the excitations about the *nodes* of a *d*-wave superconducting gap.

In QED_3 , the magnetic catalysis of the chiral symmetry breaking for strong external fields is established by looking at the Schwinger-Dyson equations [6,7]. In these works the Landau level formalism was used to truncate the fermion propagators to the lowest Landau level. This formalism is satisfactory for certain aspects of the magnetic catalysis for strong magnetic fields [7], but for weak fields the result can definitely be questioned, given that in that case the spacing between Landau levels becomes small, and one effectively deviates from the lowest Landau level description. Recently two of us [20] have looked at the rôle of higher Landau levels and showed that they contribute by inducing a (parity-violating) magnetic moment which scales with the applied magnetic field. Moreover the rôle of higher Landau levels in inducing a critical temperature even in the free fermion case, under certain circumstances, was emphasized in [8]. For all of the above reasons it is important to incorporate the effects of *all* the higher Landau levels in the Schwinger-Dyson formalism, avoiding the use of the mean field Landau level decomposition altogether. This is what we shall attempt to do in the first (analytic) part of this paper. We shall compare these results by performing some preliminary (quenched) lattice analyses in the second part of the paper. In the latter respect we have to mention that the quenched approximation for fermions employed here allows for the ladder gauge quantum fluctuations in the fermion free energy to be incorporated, but prevents the use of internal fermion loops, as the treatment of the latter requires an algorithm for treating dynamical fermions which is currently under construction.

The paper is organized as follows. In section 2 we give a brief review of the $SU(2) \times U_S(1)$ model of [13], as well as the Dirac algebra in three-dimensional spacetime with an even number of fermion flavors. In section 3 we review the Schwinger-Dyson (SD) equation for the fermion propagator in the absence of the the external magnetic field. In section 4 we present the results for the case of strong external fields, where a logarithmic scaling of the induced condensate with the external magnetic field occurs. In section 5 we present the SD equations for the weak magnetic fields ignoring the photon polarization to make contact with the lattice result presented in the second half of the paper. We show that under certain approximations, the scaling behaviour of the condensate with the external magnetic field can be found. In the next section, we attempt to go beyond the quenched approximation analytically, by including the photon polarization and modify accordingly the Schwinger-Dyson equations. The analysis becomes very complicated to be handled analytically for finite temperatures, and this is the reason why we turn to the lattice formulation of the problem in section 7, where we set up the formalism and relevant notations. In section 8 the lattice results are presented for both zero and finite temperatures; in addition, a preliminary extension of the results to the non-uniform magnetic field cases is attempted by examining the magnetic catalysis phenomenon in the case of flux tubes. This model may constitute a prototype for the study of the effects of electromagnetic vortices in condensed matter systems, which are of relevance to high-temperature superconductivity. Conclusions and outlook are presented in section 9.

II. THE MODEL AND ITS SYMMETRIES

The $SU(2) \times U(1)$ model of [21] is a toy model for dynamical electroweak gauge symmetry breaking in three dimensions, while in the context of condensed-matter systems, the $SU(2) \times U_S(1)$ model of [13] is based on a gauged *particle-hole symmetry*, via a suitable extension of the spin-charge separation [19]. The holons transform as a doublet under the $SU(2)$ (particle-hole) symmetry. In this respect the model is different from other $SU(2) \times U(1)$ spin-charge separated theories, which are based on either direct gauging of genuine spin rotation $SU(2)$ symmetries [22], or non-Abelian bosonization techniques [23,24]. The phase diagram of the model of [13], and the associated symmetry-breaking patterns, are quite different from these other models.

The three-dimensional continuum Lagrangian of the model is given (in Euclidean metric, which we use hereafter) by [21,7],

$$\mathcal{L} = -\frac{1}{4}(F_{\mu\nu})^2 - \frac{1}{4}(\mathcal{G}_{\mu\nu})^2 + \bar{\Psi}_i D_\mu \gamma_\mu \Psi_i - m \bar{\Psi}_i \Psi_i \quad (2.1)$$

where $D_\mu = \partial_\mu - ig_1 a_\mu^S - ig_2 \sigma^a B_{a,\mu}$, and $F_{\mu\nu}$, $\mathcal{G}_{\mu\nu}$ are the corresponding field strengths for an abelian (“statistical”) $U_S(1)$ gauge field a_μ^S and a non-abelian (“spin”) $SU(2)$ gauge field B_μ^a , respectively. Due to the antiferromagnetic nature of the condensed matter system the fermions Ψ_i are four-component spinors, $i = 1, \dots, N$. We note that Ψ_i may be written as

$$\Psi_i \equiv \begin{pmatrix} \Psi_{i1} \\ \Psi_{i2} \end{pmatrix}. \quad (2.2)$$

Then the Lagrangian decomposes into two parts, one for Ψ_{i1} and one for Ψ_{i2} , which will be called “fermion species” in the sequel. The presence of the even number of fermion species allows us to define chiral symmetry and parity in three dimensions [17], which we discuss below. The bare mass m term is parity conserving and has been added by hand in the Lagrangian (2.1). In the model of [13,7], this term is generated dynamically via the formation of the fermion condensate $\langle \bar{\Psi} \Psi \rangle$ by the strong $U_S(1)$ coupling. However, for our purposes, the details of the dynamical mass generation is not important and hence it will be sufficient to include a bare mass term for the holons representing the mass generated by the (strongly coupled) $U_S(1)$ interactions in the superconducting phase.

In what follows we shall ignore for simplicity the non abelian gauge group structure and concentrate only in the Abelian model in the presence of an *external* electromagnetic field, which should not be confused with the statistical abelian gauge field $U_S(1)$. The incorporation of the gauged $SU(2)$ structure leads to a much richer phase structure [25,20] and we reserve the discussion for future publication.

For even-flavour models a convenient representation for the γ_μ , $\mu = 0, 1, 2$, matrices is the reducible 4×4 representation of the Dirac algebra in three dimensions [17]:

$$\begin{aligned} \gamma^0 &= \begin{pmatrix} i\sigma_3 & \mathbf{0} \\ \mathbf{0} & -i\sigma_3 \end{pmatrix} & \gamma^1 &= \begin{pmatrix} i\sigma_1 & \mathbf{0} \\ \mathbf{0} & -i\sigma_1 \end{pmatrix} \\ \gamma^2 &= \begin{pmatrix} i\sigma_2 & \mathbf{0} \\ \mathbf{0} & -i\sigma_2 \end{pmatrix} \end{aligned} \quad (2.3)$$

where σ are 2×2 Pauli matrices and the (continuum) space-time is taken to have Euclidean signature.

As well known [17] there exist two 4×4 matrices which anticommute with γ_μ , $\mu = 0, 1, 2$:

$$\gamma_3 = \begin{pmatrix} 0 & \mathbf{1} \\ \mathbf{1} & 0 \end{pmatrix}, \quad \gamma_5 = i \begin{pmatrix} 0 & \mathbf{1} \\ -\mathbf{1} & 0 \end{pmatrix} \quad (2.4)$$

where the substructures are 2×2 matrices. These are the generators of the ‘chiral’ symmetry for the massless-fermion theory:

$$\begin{aligned} \Psi &\rightarrow \exp(i\theta\gamma_3)\Psi \\ \Psi &\rightarrow \exp(i\omega\gamma_5)\Psi. \end{aligned} \quad (2.5)$$

Note that these transformations do not exist in the fundamental two-component representation of the three-dimensional Dirac algebra, and therefore the above symmetry is valid for theories with even fermion species only.

For later use we note that the Dirac algebra in $(2+1)$ dimensions satisfy the identity:

$$\begin{aligned} \gamma^\mu\gamma^\nu &= -\delta^{\mu\nu} - \tau_3\epsilon^{\mu\nu\lambda}\gamma^\lambda \quad ; \quad \tau_3 \equiv i\gamma_3\gamma_5 = \begin{pmatrix} \mathbf{1} & \mathbf{0} \\ \mathbf{0} & -\mathbf{1} \end{pmatrix} \\ \gamma^\mu\gamma^\lambda\gamma^\mu &= \gamma^\lambda \\ \gamma^\mu\gamma^0\gamma^i\gamma^j\gamma^\mu &= -\delta^{ij}\gamma^0 - 3\tau_3\epsilon^{ij} \\ \gamma^\mu\gamma^i\gamma^j\gamma^\mu &= -3\delta^{ij} - \tau_3\gamma^0\epsilon^{ij} \\ \gamma^\mu\gamma^j\gamma^i\gamma^k\gamma^\mu &= -\delta^{ij}\gamma^k - \delta^{ik}\gamma^j + \delta^{jk}\gamma^i \end{aligned} \quad (2.6)$$

which is specific to three dimensions only. Here the Greek indices are space time indices, and repeated indices denote summation.

Parity in this formalism is defined as the transformation:

$$P : \Psi(x^0, x^1, x^2) \rightarrow -i\gamma^3\gamma^1\Psi(x^0, -x^1, x^2) \quad (2.7)$$

and it is easy to see that a parity-invariant mass term for Ψ amounts to masses with *opposite* signs between the two species [17], while a parity-violating one corresponds to masses of equal signs.

The set of generators

$$\mathcal{G} = \{\mathbf{1}, \gamma_3, \gamma_5, \Delta \equiv i\gamma_3\gamma_5\} \quad (2.8)$$

form [21,13] a global $U(2) \simeq SU(2) \times U_S(1)$ symmetry. The identity matrix $\mathbf{1}$ generates the $U_S(1)$ subgroup, while the other three form the $SU(2)$ part of the group. The currents corresponding to the above transformations are:

$$J_\mu^\Gamma = \overline{\Psi}\gamma_\mu\Gamma\Psi \quad \Gamma = \gamma_3, \gamma_5, i\gamma_3\gamma_5 \quad (2.9)$$

and are *conserved* in the *absence* of a fermionic *mass* term. It can be readily verified that the corresponding charges $Q_\Gamma \equiv \int d^2x \Psi^\dagger\Gamma\Psi$ lead to an $SU(2)$ algebra [21]:

$$\begin{aligned} [Q_3, Q_5] &= 2iQ_\Delta & [Q_5, Q_\Delta] &= 2iQ_3 \\ [Q_\Delta, Q_3] &= 2iQ_5 \end{aligned} \tag{2.10}$$

In the presence of a mass term, these currents are not conserved:

$$\partial^\mu J_\mu^\Gamma = 2m\bar{\Psi}\Gamma\Psi, \tag{2.11}$$

while the current corresponding to the generator **1** is *always* conserved, even in the presence of a fermion mass. The situation is parallel to the treatment of the $SU(2) \times SU(2)$ chiral symmetry breaking in low-energy QCD and the partial conservation of axial current (PCAC). The bilinears

$$\begin{aligned} \mathcal{A}_1 &\equiv \bar{\Psi}\gamma_3\Psi, & \mathcal{A}_2 &\equiv \bar{\Psi}\gamma_5\Psi, & \mathcal{A}_3 &\equiv \bar{\Psi}\Psi \\ B_{1\mu} &\equiv \bar{\Psi}\gamma_\mu\gamma_3\Psi, & B_{2\mu} &\equiv \bar{\Psi}\gamma_\mu\gamma_5\Psi, & B_{3\mu} &\equiv \bar{\Psi}\gamma_\mu\Delta\Psi, \quad \mu = 0, 1, 2 \end{aligned} \tag{2.12}$$

transform as *triplets* under $SU(2)$. The $SU(2)$ singlets are

$$\mathcal{A}_4 \equiv \bar{\Psi}\Delta\Psi, \quad B_{4,\mu} \equiv \bar{\Psi}\gamma_\mu\Psi \tag{2.13}$$

i.e. the singlets are the parity violating mass term, and the four-component fermion number.

We now notice that in the case where the fermion condensate \mathcal{A}_3 is generated dynamically, energetics prohibits the generation of a parity-violating gauge invariant $SU(2)$ term [26], and so a parity-conserving mass term necessarily breaks [7] the $SU(2)$ group down to a τ_3 - $U(1)$ sector [12], generated by the σ_3 Pauli matrix in two-component notation. Upon coupling the system to external electromagnetic potentials, this phase with massive fermions shows *superconductivity*. The superconductivity is strongly type II [12,7] as the Meissner penetration depth of external magnetic fields turn out to be very large,² and hence the study of the response of the system to the external electromagnetic fields is justified.

III. THE SCHWINGER-DYSON EQUATION FOR THE FERMION

QED_3 is a superrenormalizable theory which is confining in the infrared regime. Accordingly, it acts as a simple prototype for the analysis of the chiral symmetry breaking in QCD. The standard tool for investigating the chiral symmetry breaking are the celebrated Schwinger-Dyson equations. In this section, let us set up the Schwinger-Dyson equations for the fermion propagator.

The Schwinger-Dyson equation concerning the fermion propagator $S_F(p)$ (for zero bare fermion mass) is given by:

$$S_F^{-1}(p) = \gamma \cdot p - g \int \frac{d^3 k}{(2\pi)^3} \gamma^\mu S_F(k) \Gamma^\nu(k, p - k) D_{\mu\nu}(p - k) \tag{3.1}$$

where Γ^ν is the fermion-photon vertex function and $D_{\mu\nu}$ is the exact photon propagator. However, to this order, let us make the following approximations:

² The high-temperature superconducting oxides are strongly type II superconductors.

1. Use the bare vertex function, namely

$$\Gamma^\nu(k, p - k) = g\gamma^\nu, \quad (3.2)$$

so that the gap equation reads:

$$S_F^{-1}(p) = \gamma \cdot p - g^2 \int \frac{d^3 k}{(2\pi)^3} \gamma^\mu S_F(k) \gamma^\nu(k, p - k) D_{\mu\nu}(p - k) \quad (3.3)$$

2. Now, we choose the following ansatz for the *full* fermion propagator:

$$S_F^{-1}(p) = A(p)\gamma^0 p_0 + B(p)\boldsymbol{\gamma} \cdot \mathbf{p} + \Sigma(p) \quad (3.4)$$

Using this ansatz, let us now perform a trace over the gamma matrices in (3.1). This gives us the following gap equation

$$\Sigma(p) = g^2 \int \frac{d^3 k}{(2\pi)^3} \frac{\Sigma(k)}{A^2 k_0^2 + B^2 \mathbf{k}^2 + \Sigma^2(k)} \sum_\mu D_{\mu\mu}(p - k) \quad (3.5)$$

3. To further simplify the gap equation let us use the zeroth order result for the wavefunction renormalization, namely $A(p) = B(p) = 1$, which is often justified in the large N argument [17] (see however [28]) so that eq.(3.5) reads:

$$\Sigma(p) = g^2 \int \frac{d^3 k}{(2\pi)^3} \frac{\Sigma(k)}{(k_0^2 + \mathbf{k}^2 + \Sigma^2(k))} D_{\mu\mu}(p - k) \quad (3.6)$$

4. The photon propagator $D_{\mu\nu}(k)$ can be replaced by the ladder resummed propagator which can be justified in the large- N limit. The resummed propagator (in the absence of the magnetic field) is given by

$$D_{\mu\nu}(p) = \frac{(\delta_{\mu\nu} - \frac{p_\mu p_\nu}{p^2})}{p^2(1 - \Pi(p))} = \frac{(\delta_{\mu\nu} - \frac{p_\mu p_\nu}{p^2})}{p^2(1 + \frac{g^2}{8p})} \quad (3.7)$$

The gap equation thus obtained in the absence of the magnetic field can be solved using the bifurcation method [17]. There are two solutions namely,

$$\Sigma_1(p) \sim p^{-8/\pi^2 N}, \quad \Sigma_2(p) \sim p^{1-8/\pi^2 N} \quad (3.8)$$

where N is the (large) number of fermion flavours. However, it is natural to expect that these solutions will change in the presence of the external magnetic field; we will discuss this generalization in the following sections.

IV. THE DYNAMICALLY GENERATED FERMION MASS AT STRONG MAGNETIC FIELDS

As mentioned above, hereafter we consider only the abelian gauge group $U_S(1)$ in the presence of an external electromagnetic potential A_μ^{ext} , corresponding to a constant magnetic field \mathbf{B} , perpendicular to the spatial plane. The dynamics is described by the Lagrangian:

$$\mathcal{L} = -\frac{1}{4}(F_{\mu\nu})^2 + \bar{\Psi}D_\mu\gamma_\mu\Psi - m\bar{\Psi}\Psi \quad (4.1)$$

where $D_\mu = \partial_\mu - ig a_\mu^S - ieA_\mu^{ext}$. The mass m here should be viewed as an (infrared) regulator mass. In the dynamical mass generation scenario investigated below via the SD method m should be set to zero, given that the dynamics of the gauge field and the magnetic field are both responsible for the appearance of a mass in the fermion propagator. For the lattice analysis, on the other hand, the presence of an initial small ‘bare’ regulating mass $m \neq 0$ appears necessary [8].

We commence our analysis by noting that the Fourier transform $\tilde{S}_F(k)$ of the fermion propagator in the presence of a constant external magnetic field has the form [10]:

$$\tilde{S}_F(k) = \int_0^\infty ds e^{-s(k_0^2 + m^2 + \mathbf{k}^2 \frac{\tanh z}{z})} [(m + \gamma \cdot k) - (\gamma_1 k_2 - \gamma_2 k_1) \tanh z] (1 + \gamma_1 \gamma_2 \tanh z) \quad (4.2)$$

where m is the mass of the fermion, and $z = s eB$. Note that we are distinguishing between the coupling constant g for the statistical $U(1)$ gauge field and the electromagnetic charge e . The Schwinger propagator admits the following expansion in terms of the Landau levels [27]:

$$\tilde{S}_F(k) \equiv -ie^{-\frac{\mathbf{k}^2}{eB}} \sum_{n=0}^{\infty} \frac{(-1)^n D_n(k_0, \mathbf{k})}{k_0^2 + m^2 + 2enB} \quad (4.3)$$

with

$$D_n(k_0, \mathbf{k}) \equiv (m - \gamma_0 k_0) \left[(1 - i\gamma_1 \gamma_2) L_n\left(\frac{2\mathbf{k}^2}{eB}\right) - (1 + i\gamma_1 \gamma_2) L_{n-1}\left(\frac{2\mathbf{k}^2}{eB}\right) \right] + 4(\gamma \cdot \mathbf{k}) L_{n-1}^1\left(\frac{2\mathbf{k}^2}{eB}\right) \quad (4.4)$$

$$= (m - \gamma_0 k_0) \left[L_n^{-1}\left(\frac{2\mathbf{k}^2}{eB}\right) + i\tau_3 \gamma_0 \left(L_n\left(\frac{2\mathbf{k}^2}{eB}\right) + L_{n-1}\left(\frac{2\mathbf{k}^2}{eB}\right) \right) \right] + 4(\gamma \cdot \mathbf{k}) L_{n-1}^1\left(\frac{2\mathbf{k}^2}{eB}\right) \quad (4.5)$$

For QED_3 the scaling of the dynamically generated fermion mass with the external magnetic field had been discussed by Shpigin [6] and two of us [7].

Let us begin with the case when the external magnetic field is very strong. As stated in the introduction, in this case it is sufficient to truncate the fermion propagator (in the absence of the $U_S(1)$ interactions) to the lowest Landau level (4.3), so that we get:

$$S_F^{LL}(k) = -ie^{-\frac{\mathbf{k}^2}{eB}} \frac{1}{m + \gamma^0 k_0} (1 - i\gamma^1 \gamma^2). \quad (4.6)$$

As we will be dealing with the lowest Landau levels only, it is expedient to choose the ansatz for the ‘exact’ propagator for the lowest Landau level fermions to be of the form

$$S_F^{LL}(k) = -ie^{-\frac{\mathbf{k}^2}{eB}} \frac{1}{\Sigma(k) + A(k)\gamma^0 k^0} (1 - i\gamma^1 \gamma^2). \quad (4.7)$$

One can then read off the gap equation from (3.5) by setting $B(k)$ to zero and rescaling $A \rightarrow Ae^{\frac{\mathbf{k}^2}{eB}}$ and $\Sigma \rightarrow \Sigma e^{\frac{\mathbf{k}^2}{eB}}$ (the presence of the projector $\frac{1-i\gamma^1\gamma^2}{2}$ doesn't modify the gap equation as can be seen by taking the trace over the gamma matrices). Hence, the gap equation for the lowest Landau level fermion is given by

$$\Sigma(p)e^{\frac{\mathbf{p}^2}{eB}} = g^2 \int \frac{d^3 k}{(2\pi)^3} e^{-\frac{\mathbf{k}^2}{eB}} \frac{\Sigma(k)}{A^2 k_0^2 + \Sigma^2(k)} D_{\mu\nu}(p - k) \quad (4.8)$$

It is also sufficient to take the tree level photon propagator in (3.5):

$$D_{\mu\nu}^0(p) = \frac{\delta_{\mu\nu} - \frac{p_\mu p_\nu}{p^2}}{p^2} \quad (4.9)$$

This can be justified [6] by the noting that in the presence of strong magnetic fields the photon vacuum polarization gets suppressed as $\frac{1}{\sqrt{eB}}$ at strong magnetic fields.

Accordingly, we have

$$\Sigma(p)e^{\frac{\mathbf{p}^2}{eB}} = 2g^2 \int \frac{dk_0}{(2\pi)^3} \frac{\Sigma(k)}{A^2 k_0^2 + \Sigma^2(k)} \int e^{-\frac{\mathbf{k}^2}{eB}} \frac{d^2 k}{(p - k)^2} \quad (4.10)$$

Let us set p to zero. Then,

$$\Sigma(0) = 2g^2 \int \frac{dk_0}{(2\pi)^3} \frac{\Sigma(k)}{A^2 k_0^2 + \Sigma^2(k)} \int e^{-\frac{\mathbf{k}^2}{eB}} \frac{d^2 k}{k_0^2 + \mathbf{k}^2} \quad (4.11)$$

Next setting $\mathbf{k}^2 \equiv x$, we get

$$\Sigma(0) = 2g^2 \pi \int \frac{dk_0}{(2\pi)^3} \frac{\Sigma(k)}{A^2 k_0^2 + \Sigma^2(k)} \int e^{-\frac{x}{eB}} \frac{dx}{k_0^2 + x} \quad (4.12)$$

For strong fields $eB \rightarrow \infty$, we suppose that setting $\Sigma(k) \approx \Sigma(0)$ and $A \approx 1$ yield a sufficiently good approximation [28]. Then, the gap equation becomes:

$$1 = \frac{g^2}{4\pi^2} \int dk_0 \int dx e^{-\frac{x}{eB}} \frac{1}{k_0^2 + x} \frac{1}{k_0^2 + \Sigma^2(0)}. \quad (4.13)$$

Assuming that the dynamically generated fermion mass is much smaller than the external magnetic field, i.e. $\Sigma(0) \ll \sqrt{eB}$, we get the transcendental equation:

$$\Sigma(0) \approx \frac{g^2}{2\pi} \int_{\Sigma(0)}^{\sqrt{eB}} dy \frac{e^{-\frac{y^2}{eB}}}{y} \approx 2\alpha \ln \left(\frac{\sqrt{eB}}{\Sigma(0)} \right), \text{ where } \alpha \equiv \frac{g^2}{4\pi}. \quad (4.14)$$

This equation can be solved numerically as in [13].

Note that the most important aspect of this type of behavior comes from the presence of the exponential factor in the form of the free propagator in (4.6). However, when the external magnetic field is weak, one has to include all the higher Landau levels as the levels become closely spaced. Also, the wavefunctions for these levels grow with momentum as they involve Laguerre Polynomials. Hence, one has to work with a generic ansatz for the fermion propagator, such as (3.4).

V. THE DYNAMICAL FERMION MASS IN WEAK EXTERNAL MAGNETIC FIELDS UNDER QUENCHED APPROXIMATION

We are looking at the leading scaling behaviour with the magnetic field intensity of the dressed fermion propagator in the presence of an external magnetic field eB for the case of weak fields $eB \ll \Sigma(0)$ where $\Sigma(0) \equiv m$ is a dynamically generated mass due to the statistical $U_S(1)$ interactions in the model. Obviously, since $m \propto g^2$, whereas g denotes the coupling of these interactions, the weak field limit is achieved for relatively strong gauge interactions. However, as stated earlier, we are interested in the behavior of the system under weak magnetic fields as well and in this regime the Landau level decomposition is not particularly helpful.

We make the ansatz that the fermion propagator in the presence of an external magnetic field takes the form:

$$S_F^{-1}(p) = [A_0 + A_1 \gamma_1 \gamma_2] \gamma_0 p_0 + C \boldsymbol{\gamma} \cdot \mathbf{p} + [\Sigma_0 + \Sigma_1 \gamma_1 \gamma_2]. \quad (5.1)$$

We note that a propagator of this form reproduces the correct versions of the propagator in the limits of strong magnetic fields (with $A_1 = -iA_0$, $C = 0$ and $\Sigma_1 = -i\Sigma_0$; compare with equation 4.4) and weak magnetic fields (with $A_1 = \Sigma_1 = 0$, $C = A_0$). The Schwinger-Dyson equation for the fermion propagator in the massless limit assumes the form:

$$S_F^{-1}(p) = \boldsymbol{\gamma} \cdot \mathbf{p} - g^2 \int \frac{d^3 k}{(2\pi)^3} D_{\mu\nu}(p - k) \gamma^\mu S_F(k) \gamma^\nu \quad (5.2)$$

It is sufficient for our purposes to use the bare photon vertex, and set the wave-function renormalization to one. These will be justified later on.

Taking the trace in the above equation, we obtain:

$$4\Sigma(p) = -g^2 \int \frac{d^3 k}{(2\pi)^3} D_{\mu\nu}(p - k) \text{Tr}(\gamma^\mu \tilde{S}_F(k) \gamma^\nu) \quad (5.3)$$

where we denoted Σ_0 by $\Sigma(p)$. A more important remark is that inside the integral we have approximated the (unknown) fermion propagator $S_F(k)$ by the form $\tilde{S}_F(k)$ of equation 4.2, which is the propagator in a homogeneous external magnetic field. One has:

$$\begin{aligned} \text{Tr}(\gamma^\mu \tilde{S}_F(k) \gamma^\nu) &= \int_0^\infty ds e^{-s(k_0^2 + \mathbf{k}^2 \tanh z + \Sigma^2)} \text{Tr}[\gamma^\mu (\boldsymbol{\gamma} \cdot \mathbf{k} + \Sigma(k)) \gamma^\nu + \\ &\quad \gamma^\mu (\Sigma(k) + \boldsymbol{\gamma} \cdot \mathbf{k}) \gamma_1 \gamma_2 \gamma^\nu \tanh z - \gamma^\mu (\gamma_1 k_2 - \gamma_2 k_1) \tanh z (1 + \gamma_1 \gamma_2 \tanh z) \gamma^\nu] \end{aligned} \quad (5.4)$$

Since we work in the Landau gauge, $D_{\mu\nu}(q)$ is given by $\frac{q^2 \delta_{\mu\nu} - q_\mu q_\nu}{q^4}$. Using the following identities of the γ matrices in Euclidean space:

$$\begin{aligned} \text{Tr}(\gamma_\mu \gamma^\mu) &= -3 \\ (q \cdot \boldsymbol{\gamma})^2 &= -q^2 \\ \text{Tr}(\gamma^\mu \mathcal{O} \gamma^\nu) D_{\mu\nu}(q) &= -\frac{2}{q^2} \text{Tr} \mathcal{O} \end{aligned} \quad (5.5)$$

where \mathcal{O} is any operator, one can write (5.4) in the form:

$$D_{\mu\nu}(p-k)\text{Tr}\left(\gamma^\mu \tilde{S}_F(k)\gamma^\nu\right) = -\frac{8}{(p-k)^2} \int_0^\infty ds \Sigma(k) e^{-s(k_0^2 + \mathbf{k}^2 \frac{\tanh z}{z} + \Sigma^2(k))}. \quad (5.6)$$

Using (5.6), (5.3) becomes:

$$\Sigma(p) = \frac{2g^2}{(2\pi)^3} \int_0^\infty ds \int \frac{d^3 k}{(k-p)^2} \Sigma(k) e^{-s(k_0^2 + \mathbf{k}^2 \frac{\tanh z}{z} + \Sigma^2(k))} \quad (5.7)$$

Setting $p = 0$ and approximating $\Sigma(k) \simeq \Sigma(0) \equiv m$ in the integrand yields:

$$1 = \frac{2g^2}{(2\pi)^3} \int_0^\infty ds \int d^3 k \frac{1}{k_0^2 + \mathbf{k}^2} e^{-s(k_0^2 + \mathbf{k}^2 \frac{\tanh z}{z} + m^2)}. \quad (5.8)$$

Now we use the parametrization: $k_0 = k \cos\theta$, $\mathbf{k}^2 = k^2 \sin^2\theta$, and get:

$$1 = \frac{g^2}{4\pi^{\frac{3}{2}}} \int_0^\infty ds \int_{-1}^{+1} dx \frac{e^{-sm^2}}{\sqrt{s(x^2 + (1-x^2)\frac{\tanh z}{z})}}, \quad (5.9)$$

with $x \equiv \cos\theta$. Then the x integration can be performed:

$$1 = \frac{1}{4\pi^{\frac{3}{2}}} \frac{g^2}{\sqrt{eB}} \int_0^\infty dz e^{-z\frac{m^2}{eB}} \frac{1}{\sqrt{z - \tanh z}} \log \frac{\sqrt{z} + \sqrt{z - \tanh z}}{\sqrt{z} - \sqrt{z - \tanh z}}, \quad (5.10)$$

where we have set $z \equiv eBs$. At this point we define two dimensionless variables: $\mu \equiv 2\pi \frac{m}{g^2}$, $f \equiv 2\pi \frac{\sqrt{eB}}{g^2}$, and write the last equation in terms of μ and f :

$$1 = \frac{1}{2\sqrt{\pi}} \frac{1}{f} \int_0^\infty dz e^{-z\frac{\mu^2}{f^2}} \frac{1}{\sqrt{z - \tanh z}} \log \frac{\sqrt{z} + \sqrt{z - \tanh z}}{\sqrt{z} - \sqrt{z - \tanh z}}. \quad (5.11)$$

For each value of f the above relation gives a corresponding value for μ . The result is a universal curve $\mu(f)$, which we depict in the figure 3 as a dashed line. This result can be translated very easily to the language of dimensionful parameters, as well as to the lattice parameters. Notice that up to now there is no restriction to weak fields.

One may also derive an analytical approximation for the regime of weak magnetic fields. Starting from eq.(5.8) we write the term $e^{-s\mathbf{k}^2 \frac{\tanh z}{z}}$ in the form $e^{-s\mathbf{k}^2} \cdot e^{-s\mathbf{k}^2(\frac{\tanh z}{z} - 1)}$, expand the second exponential in a power series of $z = eBs$ for weak fields and retain the terms which are at most of sixth order in eB . Then the same parametrization as before is used and the integrations over k and x are similarly carried out. Then the equation involving the integral over z is replaced by:

$$1 = \frac{g^2}{2\pi} \left[\frac{1}{m} + \frac{1}{12} \frac{e^2 B^2}{m^5} - \frac{7}{48} \frac{e^4 B^4}{m^9} + \frac{773}{960} \frac{e^6 B^6}{m^{13}} + \mathcal{O}(e^8 B^8) \right] \quad (5.12)$$

For weak fields we may solve equation (5.12) by substituting the expansion $m = m_0 + m_2(eB)^2 + m_4(eB)^4 + \dots$ in (5.12) and equating the coefficients of equal powers of eB to determine the coefficients m_k . The resulting solution of (5.12) is:

$$m = \frac{g^2}{2\pi} \left(1 + \frac{4\pi^4 e^2 B^2}{3g^8} - \frac{400\pi^8 e^4 B^4}{9g^{16}} + \frac{534208\pi^{12} e^6 B^6}{135g^{24}} + \mathcal{O}(e^8 B^8) \right), \quad (5.13)$$

which may also be written as:

$$\mu = 1 + \frac{1}{12} f^4 - \frac{25}{144} f^8 + \frac{8237}{8640} f^{12} + \mathcal{O}(f^{16}). \quad (5.14)$$

The above relations show that for weak magnetic fields the dynamically generated mass is quadratic in B . For somewhat bigger magnetic fields, however, the quadratic behaviour is compensated by a negative quartic contribution and the increase with the magnetic field resembles very closely a linear dependence. Of course for even bigger magnetic fields higher order contributions take over.

Although we have already depicted in figure 3 the full solution $\mu(f)$, we also plot the solution of equation (5.12) (we note here that we did not actually use the solution (5.13), but rather the one which results if (5.12) is quenched to order B^2 before solving); this is done to gain some feeling about the accuracy of the quadratic approximation, which will be the only possible approach in the case where also dynamical fermions are taken into account. The approximate solution is the full line and is restricted in the region of small B , where it is appropriate; it is quite good up to $\sqrt{\frac{eB}{g^2}} \approx 0.1$.

As we have just seen, in the quenched approximation one uses the free photon propagator as the fermion loops (which modifies the fermion propagator) are ignored. In the next section, we examine whether the inclusion of the photon polarization modifies the scaling behaviour of the gap function with eB discussed above.

VI. BEYOND THE QUENCHED APPROXIMATION

To take into account the contribution of internal fermion loops we begin with a study of the one-loop vacuum polarization graph in QED_3 in the case of even number of fermion flavors. The polarization tensor in the one-loop approximation is given by :

$$\Pi_{\mu\nu}(p) = -g^2 \int \frac{d^3 k}{(2\pi)^3} \text{tr} \left(\gamma_\mu \tilde{S}(k) \gamma_\nu \tilde{S}(k-p) \right) \quad (6.1)$$

where $\tilde{S}(k)$ is the fermion propagator in the presence of the external magnetic field (4.2).

The calculation of the polarization tensor is straightforward. For our case, it can be obtained easily by performing a dimensional reduction of the four-dimensional result [30,31]. We end up with

$$\Pi_{\mu\nu}(p) = (p^2 \delta_{\mu\nu} - p_\mu p_\nu) N_0(p) + (p_\perp^2 \delta_{\mu\nu} - p_{\perp\mu} p_{\perp\nu}) N_1(p) \equiv p^2 P_{\mu\nu} N_0(p) + \mathbf{p}^2 P_{\perp\mu\nu} N_1(p), \quad (6.2)$$

where $\mathbf{p}^2 \equiv p_\perp^2$ with $p_{\perp\mu} = (0, p_1, p_2)$ and

$$\begin{aligned} N_0(p) &= -\frac{g^2}{8\pi^{\frac{3}{2}}} \int_0^\infty \frac{ds}{\sqrt{s}} \int_{-1}^{+1} dv e^{-s\phi_0} \frac{z}{\sinh z} [\cosh zv - v \coth z \sinh zv] \\ N_1(p) &= -\frac{g^2}{8\pi^{\frac{3}{2}}} \int_0^\infty \frac{ds}{\sqrt{s}} \int_{-1}^{+1} dv e^{-s\phi_0} \frac{2z}{\sinh^3 z} [\cosh z - \cosh zv] - N_0(p) \end{aligned} \quad (6.3)$$

with

$$\begin{aligned}\phi_0 &= m^2 + \frac{1-v^2}{4} p_0^2 + \frac{\cosh z - \cosh zv}{2z \sinh z} \mathbf{p}^2; \\ z &\equiv eBs\end{aligned}\quad (6.4)$$

An outline of the derivation of the above-mentioned formulae is provided in the appendix.

For weak magnetic fields, we will have $\sqrt{eB} \ll \Sigma(0)$, where $\Sigma(0)$ is the dynamically generated fermion mass. Note that it is the opposite to the limit encountered in the case for the strong magnetic field [6,21]. In the weak-field limit, we can expand the above functions in a power series of $z = s\Sigma^2(0) \left(\frac{eB}{\Sigma^2(0)}\right)$ and take the leading and next to leading order behavior as $z \rightarrow 0$.

We have, as $z \rightarrow 0$, the following expansions to order $e^2 B^2$:

$$\phi_0 = \Sigma^2 + \frac{1-v^2}{4} p^2 - \frac{z^2}{48} (1-v^2)^2 \mathbf{p}^2 + O(z^4), \quad (6.5)$$

$$N_0(p) = -\frac{g^2}{8\pi^{\frac{3}{2}}} \int_0^\infty \frac{ds}{\sqrt{s}} \int_{-1}^{+1} dv e^{-s\phi_0} (1-v^2) \left[1 - \frac{z^2}{6} (1-v^2) \right] + O(z^4), \quad (6.6)$$

$$N_1(p) = -\frac{g^2}{8\pi^{\frac{3}{2}}} \int_0^\infty \frac{ds}{\sqrt{s}} \int_{-1}^{+1} dv e^{-s\phi_0} \frac{z^2}{12} (-3 + 2v^2 + v^4) + O(z^4). \quad (6.7)$$

Note that when $z \rightarrow 0$ the term $N_1(p)$ vanishes and we recover the usual form for the polarization tensor.

To simplify the integrals, we also expand the exponential $e^{-s\phi_0}$ in a power series in z so that,

$$e^{-s\phi_0} \sim e^{-s(\Sigma^2 + \frac{1-v^2}{4} p^2)} \left(1 + \frac{e^2 B^2 s^3}{48} (1-v^2)^2 \mathbf{p}^2 \right) \quad (6.8)$$

This simplifies the s -integrals. We then end up with:

$$\begin{aligned}N_0(p) &= -\frac{g^2}{2\pi p} \left[\left(\frac{1}{2} - \frac{2\Sigma^2}{p^2} \right) \sin^{-1} \kappa + \frac{\Sigma}{p} \right. \\ &\quad \left. - \frac{2e^2 B^2}{p^4} \left\{ \sin^{-1} \kappa - \frac{2\Sigma \kappa^2 (3 + 2\kappa^2)}{3p} \right\} \right. \\ &\quad \left. + \frac{5e^2 B^2 \mathbf{p}^2}{2p^6} \left\{ \sin^{-1} \kappa - \frac{2\Sigma \kappa^2 (15 + 10\kappa^2 + 8\kappa^4)}{15p} \right\} \right] \quad (6.9)\end{aligned}$$

$$N_1(p) = -\frac{g^2 e^2 B^2}{2\pi p^5} \left[\sin^{-1} \kappa - p \frac{3 - \kappa^2 + 6\kappa^4}{6\Sigma} \right] \quad (6.10)$$

where $\kappa^2 \equiv \frac{p^2}{4\Sigma^2 + p^2}$. Note that for physical processes $0 \leq \kappa \leq 1$. When, $eB = 0$ and $\Sigma = 0$ (i.e. $\kappa = 1$) we recover the known results (equation 3.7), namely $N_0(p) = -\frac{g^2}{8p}$, $N_1(p) = 0$.

On the other hand, in the presence of the magnetic field one can readily see that in the limit $\Sigma \rightarrow 0$ the function $N_1(p)$ blows up when $\kappa \rightarrow 1$ (i.e. the massless case) due

to the presence of the factor Σ in the denominator. However, for a super renormalizable theory this seems unphysical. A resolution to this puzzle can be provided by the generation of a dynamical fermion mass Σ (however small) in the presence of the magnetic field. This observation points to the magnetic catalysis even in the case for the weak fields in three-dimensional QED. Generation of such a mass would prevent the appearance of the divergences.

For $\Sigma \neq 0$, $N_0(p)$ and $N_1(p)$ vanishes when $\Sigma \ll p$ and $p \rightarrow \infty$ as

$$N_0(p) \approx -\frac{g^2}{8p} \left(1 - \frac{4e^2 B^2}{p^4} + \frac{5e^2 B^2 \sin^2 \theta}{p^4} \right), \quad (6.11)$$

$$N_1(p) \approx -\frac{g^2 e^2 B^2}{2\pi p^5} \left(\frac{\pi}{2} - \frac{4p}{3\Sigma} \right) \quad (6.12)$$

where we have used the parametrization $\mathbf{k}^2 = k^2 \sin^2 \theta$, as before. Hereafter we will be using the approximations (6.11) and (6.12) which are justified in the weak-field case.

As in the case with the quenched treatment let us proceed to get the gap equation. To take account of the photon propagator, we can invoke the large-N argument to sum up the photon propagator in the ladder approximation :

$$D_{\mu\nu}(p) = D_{\mu\nu}^0(p) + D_{\mu\kappa}^0(p)\Pi_{\kappa\rho}(p)D_{\rho\nu}^0(p) + \dots \quad (6.13)$$

where $D_{\mu\nu}^0$ is the free photon propagator. To facilitate our calculations let us use the Landau gauge for the zeroth order propagator, so that

$$D_{\mu\nu}^0(p) = \frac{\delta_{\mu\nu} - \frac{p_\mu p_\nu}{p^2}}{p^2} \quad (6.14)$$

Using the algebraic properties of the projectors

$$\begin{aligned} P_{\mu\nu}(p)P_{\nu\rho}(p) &= P_{\mu\rho}(p) \\ P_{\mu\nu}(p)P_{\perp\nu\rho}(p_\perp) &= P_{\perp\nu\rho}(p_\perp) \\ P_{\perp\mu\nu}(p_\perp)P_{\perp\nu\rho}(p_\perp) &= P_{\perp\nu\rho}(p_\perp) \end{aligned} \quad (6.15)$$

we can sum the series in (6.13) to get

$$D_{\mu\nu}(p) = \frac{1}{p^2(1 - N_0(p))} \left[P_{\mu\nu} + P_{\perp\mu\nu} \frac{N_1(p) \frac{\mathbf{p}^2}{p^2}}{(1 - (N_0(p) + \frac{\mathbf{p}^2}{p^2} N_1(p)))} \right] \quad (6.16)$$

To go beyond the case of quenched approximation which we discussed in the previous section, we need to include the polarization effects in our analysis treatment. To perform this improvement we replace the photon propagator in (5.3) by the ladder resummed one, given by (6.16). For the fermion propagator we proceed as we did previously for the quenched case: starting from equation (5.4) we expand the term $e^{-s\mathbf{k}^2 \frac{\tanh z}{z}}$ and get the expression $e^{-s\mathbf{k}^2} \cdot e^{-s\mathbf{k}^2(\frac{\tanh z}{z} - 1)}$. Then we expand the second exponential in powers of $z = eBs$, retain the terms which are at most of second order in eB and integrate over s . Taking traces over the Dirac γ matrices we finally get:

$$\Sigma(p) = g^2 \int \frac{d^3 k}{(2\pi)^3} \frac{\Sigma(k)}{(k_0^2 + \mathbf{k}^2 + \Sigma^2(k))} \left(1 + \frac{2e^2 B^2 \mathbf{k}^2}{(\Sigma^2 + k^2)^3} \right) \frac{1}{(p - k)^2 (1 - N_0(p - k))} \times \\ \left[2 + \frac{N_1(p - k) \frac{(\mathbf{p} - \mathbf{k})^2}{(p - k)^2}}{(1 - (N_0(p - k) + \frac{(\mathbf{p} - \mathbf{k})^2}{(p - k)^2} N_1(p - k))} \right] \quad (6.17)$$

Let us now set $p = 0$ and as in the case of the quenched approximation let us make the substitution $\Sigma(k) \simeq \Sigma(0) \equiv m$ to get

$$1 = g^2 \int \frac{d^3 k}{(2\pi)^3} \frac{\left(1 + \frac{2e^2 B^2 \mathbf{k}^2}{(m^2 + k^2)^3} \right)}{(k_0^2 + \mathbf{k}^2 + m^2)} \frac{1}{k^2 (1 - N_0(k))} \times \\ \left[2 + \frac{N_1(k) \frac{\mathbf{k}^2}{k^2}}{(1 - (N_0(k) + \frac{\mathbf{k}^2}{k^2} N_1(k)))} \right] \quad (6.18)$$

Now as $k^2 = k_0^2 + k_\perp^2$ and we can use the parametrization $k_0 = k \cos \theta$ and $|\mathbf{k}| = k \sin \theta$. Let us write, using (6.11),

$$N_0(p) = E(p) + F(p) \sin^2 \theta \quad (6.19)$$

where $E(p) = -\frac{g^2}{8p} (1 - \frac{4e^2 B^2}{p^4})$ and $F(p) = -\frac{5g^2 e^2 B^2}{8p^5}$. Accordingly, we can rewrite (6.18) as

$$1 = g^2 \int \frac{dk}{(2\pi)^2} \frac{1}{(k^2 + m^2)} \times \int_0^\pi d\theta \frac{\sin \theta}{(1 - E(k) - F(k) \sin^2 \theta)} \\ \times \left[2 + \frac{N_1(k) \sin^2 \theta}{(1 - E_0(k) - (F(k) + N_1(k)) \sin^2 \theta)} \right] \left(1 + \frac{2e^2 B^2 k^2 \sin^2 \theta}{(m^2 + k^2)^3} \right) \quad (6.20)$$

The angular integral can be performed by making a change of variables $y = \cos \theta$, so that we end up with

$$1 = \frac{g^2}{\pi^2} \int dk \frac{1}{(k^2 + m^2)} \left[\frac{1}{F(k)} \left(\left\{ 1 + \frac{2e^2 B^2 k^2 (b^2 + 1)}{(k^2 + m^2)^3} \right\} \frac{1}{b} \tan^{-1} \left(\frac{1}{b} \right) - 2 \frac{e^2 B^2 k^2}{(k^2 + m^2)^3} \right) \right. \\ \left. + \frac{e^2 B^2 k^2 N_1(k)}{(k^2 + m^2)^3 F(k) (F(k) + N_1(k))} - \frac{1}{2(1 - E(k))} \left(\left\{ 1 + \frac{2(b^2 + 1)e^2 B^2 k^2}{(m^2 + k^2)^3} \right\} \frac{b^2 + 1}{b} \tan^{-1} \left(\frac{1}{b} \right) \right. \right. \\ \left. \left. - \left\{ 1 + \frac{2(a^2 + 1)e^2 B^2 k^2}{(m^2 + k^2)^3} \right\} \frac{a^2 + 1}{a} \tan^{-1} \left(\frac{1}{a} \right) \right) \right] \quad (6.21)$$

where $b^2 \equiv \frac{1-E-F}{F}$ and $a^2 \equiv \frac{1-E-F-N_1}{N_1+F}$.

However, this equation is difficult to handle, so we prefer instead to expand equation (6.20) in powers of $e^2 B^2$ before doing the angular integration. After some rather tedious algebraic manipulations we end up with:

$$\frac{eB}{g^4} \equiv \frac{f^2}{4\pi^2} = \sqrt{\frac{1 - A_0}{T_1 + T_2}}. \quad (6.22)$$

The quantities appearing in the right hand side are given by the following expressions:

$$A_0 = \frac{2}{\pi\mu} \int_0^\infty dx \frac{x^2}{(x^2+1)[x^2+h(\mu,x)]}, \quad (6.23)$$

$$T_1 = \frac{128\pi^3}{3\mu^5} \int_0^\infty dx \frac{x^4}{(x^2+1)^4 h(\mu,x)}, \quad (6.24)$$

$$T_2 = \frac{128\pi^3}{9\mu^6} \int_0^\infty dx \frac{12x^4 + x^6}{(4+x^2)^3 (x^2+1) [h(\mu,x)]^2}. \quad (6.25)$$

In the above expressions we have used the notations $f \equiv 2\pi \frac{\sqrt{eB}}{g^2}$ and $\mu \equiv 2\pi \frac{m}{g^2}$, already used in the previous section; moreover, we have employed the expression:

$$h(\mu, x) \equiv \frac{1}{\mu} \left[1 + \frac{x^2 - 4}{2x} \sin^{-1} \left(\frac{x}{\sqrt{x^2 + 4}} \right) \right].$$

Numerical computation of the integrals yields $\frac{m}{g^2}$ as a function of $\frac{\sqrt{eB}}{g^2}$, which can be used to produce the lower branch in figure 3. This represents the solution of the SD equations in the region of small magnetic fields. (Note that only the small- B part of the curve is depicted). We see that the dynamically generated mass in this case is substantially smaller than in the previous section. Presumably this reflects the fact that, due to the Pauli principle, the condensate tends to decrease. We note that in the quenched case the back reaction of the fermions is not really felt, so this fact has no consequences in that case.

VII. LATTICE FORMULATION

We now proceed with a description of the lattice formulation of the problem. The lattice action is given by the formulae given below.

$$S = \frac{\beta_G}{2} \sum_{x,\mu,\nu} F_{\mu\nu}(x) F^{\mu\nu}(x) + \sum_{n,n'} \bar{\Psi}_n Q_{n,n'} \Psi_{n'} \quad (7.1)$$

$$F_{\mu\nu}(x) \equiv a_\mu^S(x) + a_\nu^S(x + \mu) - a_\mu^S(x + \nu) - a_\nu^S(x)$$

$$Q_{n,n'} = \delta_{n,n'} - K \sum_{\hat{\mu}} [\delta_{n',n+\hat{\mu}}(r + \gamma_{\hat{\mu}}) U_{n\hat{\mu}} V_{n\hat{\mu}} + \delta_{n',n-\hat{\mu}}(r - \gamma_{\hat{\mu}}) U_{n-\hat{\mu}}^\dagger V_{n-\hat{\mu}}^\dagger].$$

The indices n, n' consist actually of three integers each, (n_1, n_2, n_3) , labeling the lattice sites, while μ denotes directions. r is the Wilson parameter, K the hopping parameter, $U_{n\hat{\mu}} \equiv e^{iga\alpha_{n\hat{\mu}}^S}$, $V_{n\hat{\mu}} \equiv e^{ieaA_{n\hat{\mu}}}$. $\alpha_{n\hat{\mu}}^S$ represents the statistical gauge potential and $A_{n\hat{\mu}}$ the external electromagnetic potential. $\beta_G \equiv \frac{1}{g^2 a}$ is related to the statistical gauge coupling constant in the usual way. On the other hand, we denote by e the dimensionless electromagnetic coupling constant of the external electromagnetic field. In our treatment we will use naïve fermions, so we set $r = 0$. Initially we will consider a homogeneous magnetic field; thus one should construct a lattice version of the homogeneous magnetic field. This has already been

done before in [29] in connection with the abelian Higgs model. We more or less follow them, but follow a slightly different prescription, which we describe below [8].

Since we would like to impose an external homogeneous magnetic field in the (missing) x_3 direction, we choose the external gauge potential in such a way that the plaquettes in the x_1x_2 plane equal B , while all other plaquettes equal zero. One way in which this can be achieved is through the choice: $A_3(n_1, n_2, n_3) = 0$, for all n_1, n_2, n_3 , and

$$A_1(n_1, n_2, n_3) = -\frac{B}{2}(n_2 - 1), \quad n_1 \neq N, \quad A_1(N, n_2, n_3) = -\frac{B}{2}(N + 1)(n_2 - 1), \quad (7.2)$$

$$A_2(n_1, n_2, n_3) = +\frac{B}{2}(n_1 - 1), \quad n_2 \neq N, \quad A_2(n_1, N, n_3) = +\frac{B}{2}(N + 1)(n_1 - 1). \quad (7.3)$$

where N^3 is the number of points on the (cubic) lattice. It is trivial to check out that all plaquettes starting at (n_1, n_2, n_3) , with the exception of the one starting at (N, N, n_3) , equal B . The latter plaquette equals $(1 - N^2)B = B - (N^2B)$. One may say that the flux is homogeneous over the entire x_1x_2 cross section of the lattice and equals B . The additional flux of $-(N^2B)$ can be understood by the fact that the lattice is a torus, that is a closed surface, and the Maxwell equation $\nabla \cdot \mathbf{B} = 0$ implies that the magnetic flux through the lattice should vanish. This means that, if periodic boundary conditions are used for the gauge field, the total flux of any configuration should be zero, so the (positive, say) flux B , penetrating the majority of the plaquettes, will be accompanied by a compensating negative flux $-(N^2B)$ in a single plaquette. This compensating flux should be “invisible”, that is it should have no observable physical effects. This is the case if the flux is an integer multiple of 2π : $N^2B = m2\pi \rightarrow B = m\frac{2\pi}{N^2}$, where m is an integer. Thus we may say (disregarding the “invisible” flux) that the magnetic field is homogeneous over the entire cross section of the lattice.³ The integer m may be chosen to lie in the interval $[0, \frac{N^2}{2}]$, with the understanding that the model with integers m between $\frac{N^2}{2}$ and N^2 is equivalent to the model with integers taking on the values $N^2 - m$, which are among the ones that have already been considered. It follows that the magnetic field strength B in lattice units lies between 0 and π . The physical magnetic field B_{phys} is related to B through $B = e\alpha^2 B_{phys}$, and the physical field may go to infinity letting the lattice spacing α go to zero, while B is kept constant.

An important remark is that the magnetic field is not allowed to be too big in lattice units, since then the perturbative expansion of the expressions $e^{ieaA_{n\mu}}$ would yield significant B^2, B^3, \dots contributions with the accompanying vertices, in addition to the desirable terms which are linear in B . A trivial estimate of the critical field strength is obtained from the demand that the cyclotron radius corresponding to a given magnetic field should not be less than (say) two lattice spacings. This trivial calculation yields $B < \frac{\pi}{8}$. Of course the above limitations apply strictly only to the case where the statistical gauge field has been turned off; in the “interacting” case, one does not really know whether there exists a critical magnetic field, after which discretization effects are important. With this remark in mind, we depict in the figures of the following sections the results for the whole range of the magnetic field, from 0 to π .

³To check this translational invariance we measured the fermion condensate at every point in the x_1x_2 plane. The results were the same at all points within the error bars, confirming homogeneity.

For the fermion fields we used antiperiodic boundary conditions in the time direction and “fixed” boundary conditions in the spatial directions; the latter boundary conditions mean that we consider fermion fields vanishing on the boundaries.

VIII. LATTICE RESULTS

A. Zero Temperature Results

We are now going to present the results pertaining to the $T = 0$ case. The first set consists of measurements of the fermion condensate versus the magnetic field for a 16^3 lattice in the strong coupling regime for the statistical gauge field ($\beta_G = 0.10$) for three values of the bare mass (figure 4). Before going on with the specific features of this results, let us remark that to facilitate comparison with the analytic results we measured the magnetic field in units of its maximal value: thus we used the parameter b , defined by: $b \equiv \frac{B}{B_{max}} = \frac{eB_{phys}a^2}{eB_{phys}a^2|_{max}}$. Since $B_{max} = \pi$, as explained previously, we get: $b = \frac{B}{\pi}$ and b runs from 0 to 1. We see in figure 4 that for all three masses the plot consists of two parts with qualitatively different behaviour. For b smaller than about 0.3 we find a dependence of the condensate on the external magnetic field, which is nearly linear, however, in view of the analytical results obtained in section 5 about the quenched case, we understand that we see the quadratic behaviour found there; however, there is a negative quartic term coming into the game, as we also saw, and this “straightens out” the quadratic curve and makes it almost linear. For big magnetic fields we find points that could possibly be fitted to a logarithmic type of curve. The logarithmic dependence

$$\frac{\Sigma(0)}{\alpha} \simeq \ln \left[\frac{\sqrt{eB}}{\alpha} \right], \quad \alpha \equiv \frac{g^2}{4\pi},$$

has been found [13] by an approximate solution of the Schwinger-Dyson equations in the regime of strong magnetic fields. We have included such a logarithmic fit for $m = 0.050$ in figure 4. In addition, for this mass some points in the intermediate region are included. They show a smooth interpolation between the two regions. Thus in both the strong and weak magnetic field regimes we find a nice qualitative agreement of the analytical solutions with the Monte Carlo results. In the figure we have also included the extrapolation to the zero mass limit.

The magnetic field has been characterized as “strong” or “weak” through its comparison with the fine structure constant $\alpha \equiv \frac{g^2}{4\pi}$ and the dynamically generated mass $m \simeq \Sigma(0)$. Since figure 4 contains the strong coupling data, it would be interesting to explore the fate of the whole picture shown in figure 4 as the gauge coupling g moves away from the strong coupling regime. One would naively expect that the magnetic fields will be more easily characterized as “strong”, as compared to the smaller and smaller scale set by the gradually weaker coupling constant. Thus, the almost linear part should be restricted to the very small magnetic fields and eventually disappear. This is what one may see in figure 5, which is similar to figure 4, the only difference being that the gauge coupling constant is now in the intermediate coupling regime, rather than the strong coupling of figure 4. We see that

the almost linear part is now restricted in the region between $b = 0$ and $b \approx 0.12 - 0.15$. We may also have a semi-quantitative estimate of the new “critical” magnetic field b_c , defined as the maximum b which fits into the almost linear behaviour. Inspired by the inequality $eB \ll (\frac{g^2}{4\pi})^2$, let us suppose that $eB_c = x(\frac{g^2}{4\pi})^2$, with x a very small number; we also make the further assumption that x does not depend on g . We will check crudely whether this assumption is reasonable given our results. Converting everything to lattice units, we find that $b_c = \frac{x}{16\pi^3} \frac{1}{\beta_G^2}$. From this we infer $b_{c2} = b_{c1} \left(\frac{\beta_{G1}}{\beta_{G2}}\right)^2$. Using $\beta_{G1} = 0.10$, $\beta_{G2} = 0.15$ and $b_{c1} = 0.3$, we find for b_{c2} , the value 0.13, which is surprisingly close to the value given by the data of figure 5. Of course, the $\frac{1}{\beta_G^2}$ dependence of b_c tells us that the weak field behaviour will be even more suppressed as we move towards the weak gauge coupling; this is what we have seen in direct simulations in this regime. Thus, it is plausible that the dependence of the “critical” magnetic field has a $\frac{1}{\beta_G^2}$ dependence.

We now make contact with the results of [8], where we studied the model with the statistical gauge field turned off. We had found there that for big enough b the condensate stopped showing a monotonous increase with b , at $b = 0.5$ it had a local minimum and then had a succession of maxima and minima, up to $b = 1$. Moreover, there was a spectacular volume dependence. One expects, of course that this “free” case will be reached for big enough β_G . In figure 6 we show the results for $\beta_G = 0.5$ and $\beta_G = 1.0$ for various volumes. For $\beta_G = 0.5$ the curve shows the first sign of non monotonous behaviour at $b = 0.5$, while at $\beta_G = 1.0$ the succession of maxima and minima is clear. However, there is no detectable volume dependence, so we can be sure that, even at this large β_G , the limit of switching the gauge field off has not yet been reached; it will presumably be reached for even bigger values of β_G . One should add that in the “free” case the role of the bare mass is very important, since it is eventually the only source of mass generation. This is at the root of the large volume dependence showing up in the “free” case: at fixed volume the condensate goes over to zero for vanishing bare mass. In the full model, though, the interaction with the gauge field generates a dynamical mass, independently from the value of the bare mass. This is why in the “interacting” case the volume dependence is small, permitting a smooth transition to the thermodynamic, as well as to the massless, limit.

The simulations are done at finite values for the (bare) mass; the massless limit is taken by extrapolating the results for several bare masses to the limit $m \rightarrow 0$. Figure 7 shows the process of this extrapolation for three values of the gauge coupling constant. The external magnetic field has been set equal to a typical value ($b = 0.188$); the picture is similar for all values of the magnetic field strength. For $\beta_G = 0.10$, which lies in the strong coupling region, the extrapolation is linear with negative slope. This line is pointing to a relatively big value for the condensate in the chiral limit. For somewhat weaker coupling ($\beta_G = 0.20$), the curve is still a straight line, but the slope is positive and it points to a smaller value at $m \rightarrow 0$. In both of these cases the mass dependence is not very pronounced, because it is the strong gauge coupling which dominates in the formation of the condensate. In the third case ($\beta_G = 0.35$), which lies in the weak coupling, one can no longer fit to a straight line; a quadratic fit has proved necessary for all β_G values smaller than 0.2.

Figure 8 contains the zero mass limit of the condensate (obtained through the procedure illustrated in figure 7) versus β_G , for four values of the external field. We observe that in the strong coupling region the b -dependence of the condensate is rather weak; on the contrary,

at weak coupling, the external field is the main generator of the condensate, and we find an increasingly big b -dependence, as we move to large β_G . Note that the biggest value of b we have used in systematic measurements, such as the ones in figure 8, is 0.3. This takes into account that for larger values of b the function of the condensate stops being monotonous for large β_G , as may be seen on figure 6. Thus we have restricted our study to a b region which is safe for all values of the coupling. From this preliminary quenched study we conclude that a non-vanishing value for $\langle \bar{\Psi} \Psi \rangle$ develops for this small volume even at weak coupling in the presence of an external magnetic field. We have not tried to study systematically the approach to the continuum limit.

B. Finite Temperature Results

We expect that the fermion condensate, generated by any mechanism (explicit mass term, gauge interactions, external fields) should vanish at high temperatures. This is the study we now turn to: we employ asymmetric lattices and consider the behaviour of the condensate versus β_G . Before describing the behaviour of the condensate, let us first see the β_G dependence of the Wilson line.

Figure 9 depicts the Wilson line versus β_G for lattices of temporal size $N_\tau = 4$ and various spatial volumes. We observe in the figure not only the decrease of the Wilson line with increasing spatial volume, but also the fact that initially this quantity is almost independent of β_G , but at $\beta_G \simeq 0.25$ its dependence on β_G starts showing up. It is important that this value of β_G is independent from the spatial volume.

In figure 10 we show the relationship between Wilson lines on lattices with $N_\tau = 2$ versus $N_\tau = 4$ and $N_\tau = 6$. The result for the $16^2 * 6$ lattice lies “below” the result for the $16^2 * 4$. This is due to the fact that the former lattice is closer to the zero temperature (symmetric) lattices, as compared to the latter. The value of β_G , above which there is β_G dependence is substantially bigger for $N_\tau = 6$ than for $N_\tau = 4$ or $N_\tau = 2$. The Wilson line for the $N_\tau = 2$ case approaches an asymptotic value for large β_G . This is not very obvious in the other two cases, because they lie farther from the infinite temperature limit. Also in this case the statistical fluctuations are very large, resulting in big errors. With this in mind we have put in the figure only the errors for the case $N_\tau = 2$.

Figure 11 contains the zero (bare) mass extrapolations for the condensate as a function of β_G . The external magnetic field is set to $b = 0.1$. The uppermost curve contains the results for a symmetric lattice (16^3 .) It is easily seen that it is a quite smooth curve and presents no apparent discontinuities of any sort. The data for the asymmetric lattice $16^2 * 4$ follow the ones of the symmetric lattice at strong coupling; in the weak coupling region the condensate for the asymmetric lattice appears substantially smaller than its 16^3 counterpart. This is what one should explain on account of the symmetry restoration scenario at finite temperatures. The $16^2 * 4$ data can be described by two branches, one containing the strong and the other the weak coupling results; the two branches join at about $\beta_G = 0.4$, but their slopes do not coincide. There is a discontinuity at this value of β_G , which we interpret as the symmetry restoring transition at finite temperature. On the same figure we have put the results for a lattice of bigger spatial volume ($24^2 * 4$), away from the “critical” $\beta_G = 0.4$ value. These data do not differ substantially from the ones for $16^2 * 4$.

Figure 12 contains results similar to the ones of figure 11, but the value of the external magnetic field differs: $b = 0.305$. The same basic picture appears here, as well: we may again spot the discontinuity at $\beta_G = 0.4$ for $N_t = 4$. In addition to the data of figure 11 we have put the data for a $24^2 * 6$ lattice, which is expected to lie closer to zero temperature. The data are smoother than the ones for $16^2 * 4$ and they lie much closer to the 16^3 results; this makes it more difficult than before to spot a sudden change in slope; however, this change is present even in this case. The new element here is the data for $N_t = 2$. The change in slope here is very pronounced and substantiates our claim that we have a phase transition around $\beta_G = 0.4$.

Since we now have data for several asymmetric lattices, we are in a position to show the temperature dependence of the condensate. This is done in figure 13, in the weak coupling regime, for two values of the magnetic field. The zero mass extrapolation of the results has been used and the temperature in lattice units is $\frac{1}{N_t}$, as usual. We observe the fall of the condensate at high temperatures, which is more dramatic for the smallest value of b . This figure is of the same qualitative form with figure 2 of [8], which was derived analytically for the case where we had no statistical gauge field at all.

In figure 14 we show the time evolution of the condensate for two values of the magnetic field at weak coupling for a symmetric lattice. The important feature here is the very small magnitude of the statistical fluctuations, resulting in relatively small errors.

The situation in figure 14 changes in the asymmetric lattices and the results of figure 14 should be contrasted against the ones in figures 15 and 16. In figure 15 we have exactly the same parameters as in figure 14, however now we have a $16^2 * 4$ lattice. It is evident that the fluctuations have grown about one order of magnitude larger.

The statistical fluctuations grow even larger for the $16^2 * 2$ lattice, whose results are shown in figure 16. Moreover, this figure gives a feeling of the way the average of the condensate is approaching zero at high enough temperatures. The outcome spends most of its time at small values and has some exceptional big spikes from time to time; these latter become more and more rare as the spatial volume increases.

C. Non-uniform Magnetic Field

In the previous sections we have considered the case of a uniform external magnetic field. There is however potential physical interest in the effects of non-uniform fields, which become important in case the above model has relevance to the physics of high-temperature superconductors. Indeed, it will be of interest to examine the effect of electromagnetic vortex lines on the induced fermion (holon) condensate at the nodes of d -wave superconducting gaps [7]. A simple-minded model for such vortex lines could be that of flux tubes of magnetic field. The full problem would be to take into account interactions among the flux tubes, which could shed light also in the confining aspects of the gauge groups in three dimensions. It is only by lattice methods that one may treat the problem, in view of the very big computational difficulties in the analytical approach. In this first treatment of the problem we switch off the fluctuating statistical gauge field and consider the response of the fermions to the background field only. A full treatment of the problem, including the statistical gauge interactions is left for the future.

Let us describe the technical procedure to construct a non-uniform magnetic field on the lattice. We will consider $M \times M$ plaquettes parallel to the x_1x_2 plane, around the center of the lattice, which will be penetrated by magnetic flux equal to B each. The remaining plaquettes will not carry any flux. Then we are going to measure the condensate at the center $(\frac{N}{2}, \frac{N}{2}, \frac{N}{2})$ and along a line passing through it and consisting of the sites $(\frac{N}{2}, \frac{N}{2} + 1, \frac{N}{2})$, $(\frac{N}{2}, \frac{N}{2} + 2, \frac{N}{2}), \dots, (\frac{N}{2}, N, \frac{N}{2})$.

The fact remains that the total flux through the lattice should be zero, because of $\text{div} \mathbf{B} = 0$. Thus, for each flux B penetrating a given plaquette, there should be an opposite flux somewhere else in the lattice. To construct the magnetic field that we mentioned above, we followed the strategy to build it up plaquette by plaquette taking care that we put the compensating opposite flux through the plaquette starting at the point (N, N, n_3) . If we already have a configuration of gauge potentials on a lattice, the procedure to add a plaquette of flux B at the plaquette at (N_1, N_2, n_3) (with the corresponding compensating flux $-B$ at (N, N, n_3)), consists of adding to the preexisting links the quantities denoted by ΔA_k below. $\Delta A_3(n_1, n_2, n_3)$ is set to zero for all values of the integers n_1, n_2, n_3 . ΔA_1 and ΔA_2 are also set to zero, except for the links where an explicit different statement is made. For the plaquette starting at the site (N_1, N_2, n_3) , $N_1 \neq N, N_2 \neq N$, we choose:

$$\Delta A_1(N_1, n_2, n_3) = -B, \quad n_2 = N_2 + 1, N_2 + 2, \dots, N, \quad n_3 = 1, \dots, N$$

$$\Delta A_2(n_1, N_2, n_3) = +B, \quad n_1 = N_1 + 1, N_1 + 2, \dots, N, \quad n_3 = 1, \dots, N$$

For $N_1 = N$ we impose:

$$\Delta A_1(N, n_2, n_3) = -B, \quad n_2 = N_2 + 1, N_2 + 2, \dots, N, \quad n_3 = 1, \dots, N$$

$$\Delta A_2(n_1, n_2, n_3) = 0 \quad \text{everywhere},$$

while for $N_2 = N$:

$$\Delta A_1(n_1, N, n_3) = 0 \quad \text{everywhere},$$

$$\Delta A_2(n_1, N, n_3) = B, \quad n_1 = N_1 + 1, N_1 + 2, \dots, N, \quad n_3 = 1, \dots, N$$

In the following we consider the model with the statistical gauge field turned off. We start with vanishing gauge potentials everywhere on the lattice, go through the plaquettes in the central region and add the above ΔA_k quantities to the corresponding links. In this way we end up with the flux B in the central plaquettes and the compensating flux for all the plaquettes at (N, N, n_3) . The flux through these latter plaquettes should be “invisible”, as explained in section , so B must take the values $\frac{2\pi}{M^2}n$, $n = 0, 1, \dots, \frac{M^2}{2}$.

In figure 17 we show the results for a central region of non-vanishing flux of extent 6×6 . More specifically, for the 16^3 lattice we have been using, the region with constant non-zero flux contains the plaquettes starting at (n_1, n_2, n_3) , with $6 \leq n_1 \leq 11$ and $6 \leq n_2 \leq 11$, while n_3 takes all values. Note that nothing depends on the value of n_3 . The uppermost curve in the figure depicts the result for the condensate at the site $(9, 9, 9)$. The remaining curves represent the corresponding results for the sites $(9, 12, 9)$, and $(9, 16, 9)$. The curves with $n_2 = 10, n_2 = 11$ are quite similar to the $n_2 = 9$ curve. The first substantial change takes place at the site $(9, 12, 9)$, which lies exactly on the boundary of the above region. The remaining curves dive together to a value which is accounted for by the explicit mass

term and has very little to do with the external magnetic field. Thus, we find a drop in the condensate value taking place exactly on the boundary of the central region.

To visualize the fall of the condensate on the boundary, we fixed the b parameter to 0.188 (a typical value) and plotted the value of the condensate along a straight line passing from the center of the lattice. We find the symmetric bell-shaped plot shown in figure 18.

IX. CONCLUSIONS

In this work we have studied in detail, by means of analytic and lattice methods, the phenomenon of magnetic catalysis in even-flavour QED_3 , namely the magnetic induction of a chiral-symmetry breaking fermion condensate as a result of the influence of an external magnetic field. We have shown that the scaling behaviour of the induced condensate with the external field varies according to the strength of the latter. In the weak-field regime, there is a quadratic increase of the condensate with increasing external field, to be contrasted with the logarithmic scaling behaviour in the regime of strong external magnetic fields. However, it seems that the transition from weak to strong fields is smooth, at least as far as the induced condensate is concerned, and we would characterise it as a *cross-over* rather than a phase transition at some critical value of the external field. This constitutes a prediction of the gauge theory, and it may be tested in experiments of relevance to high-temperature superconducting materials. It would be interesting to repeat the (lattice) computations for the case of four-fermion contact interactions to check on this behaviour. This would differentiate between the two models as possible candidates for the *nodal* spin-charge excitations in d -wave high-temperature superconductors [7,16].

In addition to the uniform external field case, we have also presented preliminary quenched lattice results in the case of flux tubes of magnetic field. This situation might also be of relevance to realistic situations in high-temperature superconductors, as being related to the effects of electromagnetic vortex lines on the opening of a fermion gap at the nodes of the superconductor, within the context of the gauge theory approach [7]. Our results in the non-uniform magnetic field case have indicated that the fermion chiral condensate is non zero and scales with the magnetic field of the flux tube at the core of the latter, but decays very fast outside the tube. Our considerations did not properly take into account interactions among flux tubes. The latter is an important issue, which might also bear some relation with the issue of confinement of the three-dimensional theory. We expect that a proper treatment of this problem will become available only upon the use of dynamical fermions on the lattice.

Another important issue we would like to address for future work is the computation of thermal conductivities in the context of the model of section 2, used in our simulation of the physics of planar high-temperature superconductors. As discussed in [15] there are scaling differences of the thermal conductivity between the gauge (QED_3) and four-fermion models, which would be important to analyse in detail in the context discussed in this work for comparison with experiments of high-temperature superconductors [14]. At present, the analysis of the thermal conductivity has been performed in the real time formalism [16,15], and the extension to a lattice analysis is not trivial. We hope to return to this important issue in a future publication.

ACKNOWLEDGEMENTS

We wish to thank A. Campbell-Smith for useful discussions. A.M. would like to thank M. Hott for providing ref. [31]. K.F., G.K. and N.E.M. thank S.Hands for useful discussions. K.F and G.K also thank G.Tiktopoulos for useful comments on several aspects of this work. The work of N.E.M. is partially supported by P.P.A.R.C. (U.K.) under an advanced fellowship, and that of A.M. by P.P.A.R.C. (U.K.). K.F. and G.K. would like to thank the EU for financial support (TMR project, contract no.: FMRX-CT97-0122).

APPENDIX A: CALCULATION OF THE ONE-LOOP VACUUM POLARIZATION IN THE PRESENCE OF THE EXTERNAL MAGNETIC FIELD

The photon polarization tensor for QED in the presence of the electromagnetic field was first performed by Tsai [30,31]. Here, for the sake of completeness, we outline his calculations but we will work in three-dimensions instead of four-dimensions.

Let us begin with the one-loop vacuum polarization graph (2). The polarization tensor to this approximation is given by

$$\Pi_{\mu\nu}(p) = -g^2 \int \frac{d^3k}{(2\pi)^3} \text{tr} \left[\gamma^\mu \tilde{S}(k) \gamma^\nu \tilde{S}(p-k) \right] \quad (\text{A1})$$

where the Fermion propagator is the one in the presence of the constant external magnetic field [10]

$$\begin{aligned} \tilde{S}_F(k) &= \int_0^\infty ds e^{-s(k_0^2 + m^2 + \mathbf{k}^2 \frac{\tanh z}{z})} [(m + \gamma \cdot k) - (\gamma_1 k_2 - \gamma_2 k_1) \tanh z] (1 + \gamma_1 \gamma_2 \tanh z) \\ &= \int_0^\infty ds e^{-s(m^2 + k_0^2 + \mathbf{k}^2 \frac{\tanh z}{z})} ((m + \gamma_0 k_0)(1 + \gamma_1 \gamma_2 \tanh z) + (\boldsymbol{\gamma} \cdot \mathbf{k}) \frac{1}{\cosh^2 z}) \end{aligned} \quad (\text{A2})$$

where $z \equiv eBs$. Accordingly, (A2) leads us to

$$\begin{aligned} \Pi_{\mu\nu}(p) &= -g^2 \int \frac{d^3k}{(2\pi)^3} \int_0^\infty ds_1 \int_0^\infty ds_2 e^{-(\chi_0(s_1, k) + \chi_0(s_2, p-k))} \\ &\quad \times \text{tr} \left[\gamma^\mu ((m + \gamma_0 k_0)(1 + \gamma_1 \gamma_2 \tanh z_1) + (\boldsymbol{\gamma} \cdot \mathbf{k}) \frac{1}{\cosh^2 z_1}) \right. \\ &\quad \left. \gamma^\nu ((m + \gamma_0(p-k)_0)(1 + \gamma_1 \gamma_2 \tanh z_2) + (\boldsymbol{\gamma} \cdot (\mathbf{p} - \mathbf{k})) \frac{1}{\cosh^2 z_2}) \right] \end{aligned} \quad (\text{A3})$$

where $z_i = eBs_i$, $i = 1, 2$ and

$$\chi_0(s, k) \equiv s(m^2 + k_0^2 + \mathbf{k}^2 \frac{\tanh z}{z}) \quad (\text{A4})$$

Let us now make the change of variables

$$s_1 \equiv \frac{1-v}{2}s, \quad s_2 = \frac{1+v}{2}s, \quad (\text{A5})$$

with $s \in [0, \infty)$ and $v \in [-1, 1]$. Accordingly, we get

$$\chi_0(s_1, k) + \chi_0(s_2, p - k) = s[\phi_0(p) + \phi_1(p, k)] \quad (\text{A6})$$

with

$$\begin{aligned} \phi_0(p) &\equiv m^2 + \frac{1 - v^2}{4} p_0^2 + \frac{\cosh zv - \cosh z}{2z \sinh z} \mathbf{p}^2 \\ \phi_1(p, k) &\equiv (k_0 - \frac{1 + v}{2} p_0)^2 + \frac{\tanh z_1 + \tanh z_2}{z} \left(\mathbf{k} - \frac{\tanh z_2}{\tanh z_1 + \tanh z_2} \mathbf{p} \right)^2 \end{aligned} \quad (\text{A7})$$

The loop integrals can then be performed very easily via standard Gaussian integrations some of which are listed below:

$$I_0 \equiv \int \frac{d^3 k}{(2\pi)^3} e^{-s\phi_1(p, k)} = \frac{1}{(4\pi s)^{\frac{3}{2}}} \frac{z}{\sinh z} \cosh z_1 \cosh z_2 \quad (\text{A8})$$

$$\int \frac{d^3 k}{(2\pi)^3} e^{-s\phi_1(p, k)} k_0 = \frac{1 + v}{2} p_0 I_0 \quad (\text{A9})$$

$$\int \frac{d^3 k}{(2\pi)^3} e^{-s\phi_1(p, k)} \mathbf{k} = \frac{\tanh z_2}{\tanh z_1 + \tanh z_2} \mathbf{p} I_0 \quad (\text{A10})$$

$$\int \frac{d^3 k}{(2\pi)^3} e^{-s\phi_1(p, k)} k_0 \mathbf{k} = \frac{1 + v}{2} \frac{\tanh z_2}{\tanh z_1 + \tanh z_2} I_0 p_0 \mathbf{p} \quad (\text{A11})$$

$$\int \frac{d^3 k}{(2\pi)^3} e^{-s\phi_1(p, k)} k_i k_j = \left[\left(\frac{\tanh z_1}{\tanh z_1 + \tanh z_2} \right)^2 p_i p_j - \frac{z}{s(\tanh z_1 + \tanh z_2)} \delta_{ij} \right] \quad (\text{A12})$$

We will also need the following identity for the gamma matrices:

$$\begin{aligned} \text{tr} [(1 - i\gamma_1 \gamma_2 \tanh z) \gamma_\mu \gamma_\nu] &= -4(\delta_{\mu\nu} - \tanh z(\delta_1^\mu \delta_2^\nu - \delta_1^\nu \delta_2^\mu)) \\ &= -4(\delta_{\mu\nu} - \tanh z \frac{F_{\mu\nu}}{B}) \end{aligned} \quad (\text{A13})$$

where $F_{\mu\nu}$ is the covariant representation of the external magnetic field strength. The other traces can also be evaluated by the use of the Dirac algebra (2.6).

Putting everything together [30,31] one gets (after an integration by parts)

$$\Pi_{\mu\nu}(p) = \frac{g^2}{\sqrt{2\pi}} \int \frac{ds}{\sqrt{s}} \frac{dv}{2} \frac{z}{\sinh z} e^{-s\phi_0} I_{\mu\nu} \quad (\text{A14})$$

where

$$I_{\mu\nu} = [(\delta_{\mu\nu} p^2 - p_\mu p_\nu) R_0(p) + (\delta_{\mu\nu}^\perp p_\perp^2 - p_{\perp\mu} p_{\perp\nu}) R_1(p)] \quad (\text{A15})$$

with

$$R_0(p) = (\cosh zv - v \coth z \sinh zv) \quad (\text{A16})$$

$$R_1(p) = \frac{2}{\sinh^2 z} [\cosh z - \cosh zv] - R_0(p) \quad (\text{A17})$$

Note that, unlike its four-dimensional counterpart, the vacuum polarization tensor in three dimensions is not divergent and there is no need add any counterterms. One can see this by checking the absence of poles at $s \rightarrow 0$, which is the place where poles usually show up in proper time methods.

REFERENCES

- [1] V.P. Gusynin, V.A. Miransky and I.A. Shovkovy, Phys. Rev. **D 52** (1995) 4718; Nucl. Phys. **B 462**(1996) 249.
- [2] C.N. Leung, Y.J. Ng and A.W. Ackley, Phys. Rev. **D54** (1996), 4181.
D.S. Lee, C.N. Leung and Y.J. Ng, Phys. Rev. **D 55** (1997) 6504.
V.P. Gusynin and I.A. Shovkovy, Phys. Rev. **D 56** (1997) 5456.
V.P. Gusynin, hep-ph/9709339.
- [3] I. V. Krive and S.A. Naftulin, Phys. Rev. **D46** (1992) 2737; K.G. Klimenko, Theor. Math. Phys. **89** (1992), 1161; Z. Phys. **C54** (1992) 323.
- [4] D.K. Hong, Y. Kim and S.J. Sin, Phys. Rev. **D 54** (1996) 7879.
- [5] D.K. Hong, Phys. Rev. **D57** (1998) 3759.
- [6] A. V. Shpargin, hep-ph/9611412.
- [7] K. Farakos and N.E. Mavromatos, Int. J. Mod. Phys. **B12** (1998), 809.
- [8] K. Farakos, G. Koutsoumbas and N.E. Mavromatos, Phys. Lett. **B431** (1998), 147.
- [9] V.P. Gusynin, D.K. Hong and I.A. Shovkovy, hep-th/9711016.
- [10] J. Schwinger, Phys. Rev. **82** (1951) 664.
- [11] B. Rosenstein, B. J. Warr, and S. H. Park, Phys. Rev. Lett. **62** (1989), 1433; Phys. Rep. **205** (1991) 59.
- [12] N. Dorey and N.E. Mavromatos, Phys. Lett. **250B** (1990) 907; Nucl. Phys. **B386** (1992) 614;
For a comprehensive review of this approach see: N.E. Mavromatos, Nucl. Phys. B (Proc. Suppl.) **C33** (1993)145.
- [13] K. Farakos and N.E. Mavromatos, Phys. Rev. **B57** (1998) 3017.
- [14] K. Krishana et. al. Science **277** (1997) 83.
- [15] K. Farakos, G. Koutsoumbas, and N.E. Mavromatos, Int J. Mod. Phys. **B12**, 2475 (1998).
- [16] G.W. Semenoff, I.A. Shovkovy and L.C.R. Wijewardhana Mod. Phys. Lett. **A13** (1998), 1143.
- [17] R. D. Pisarski, Phys. Rev. **D29** (1984) 2423;
T. W. Appelquist, M. Bowick, D. Karabali and L. C. R. Wijewardhana, Phys. Rev. **D33** (1986) 3704.
T. W. Appelquist, D. Nash and L. C. R. Wijewardhana, Phys. Rev. Lett. **60** (1988) 2575.
- [18] I.J.R. Aitchison and N.E. Mavromatos, Phys. Rev. **B39** (1989) 6544; *ibid* **B53** (1996), 9321.
- [19] P. W. Anderson, Science **235** (1987) 1196.
- [20] N.E. Mavromatos and A. Momen, *Mod. Phys. Lett. A13* (1998) 1765.
- [21] K. Farakos, G. Koutsoumbas and G. Zoupanos, Phys. Lett. **B249** (1990), 101.
- [22] P.W. Wiegmann, Progr. Theor. Phys. Suppl. 107 (1992), 243;
X.G. Wen and P.A. Lee, Phys. Rev. Lett. 76 (1996), 503.
- [23] J. Frohlich and P. Marchetti, Phys. Rev. **B46** (1992), 6535;
J. Frohlich, T. Kerler and and P. Marchetti, Nucl. Phys. **B374** (1992), 511.
- [24] P. A. Marchetti, Zhao-bin Su, and Lu Yu, Nucl.Phys. B482 (1996) 731.
- [25] K. Farakos, N.E. Mavromatos and D. McNeill, Phys. Rev. **D59** (1999), 034502.

- [26] C. Vafa and E. Witten, Comm. Math. Phys. **95**(1984)257.
- [27] A. Chodos, K. Everding and D. Owen, Phys. Rev. **D 42** (1990) 2881.
- [28] for recent work on the effects of wave-function renormalization see: I.J.R. Aitchison, N.E. Mavromatos, and D. McNeill, Phys. Lett. **B402** (1997), 154; K-I. Kondo and T. Murakami, Phys. Lett. **B410** (1997), 257, and references therein.
- [29] P.H.Damgaard and Urs M.Heller, Nucl.Phys. **B 309** 625 (1988).
- [30] W. Tsai, Phys. Rev. **D 10** (1974) 1399.
- [31] W. Dittrich and M. Reuter, *Effective Lagrangian in Quantum Electrodynamics*, Springer-Verlag, Berlin (1984).

FIGURES

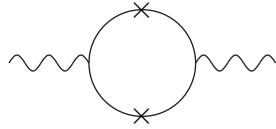


FIG. 1. One-loop vacuum polarization for photons (wavy lines) in QED_3 . The solid lines with crosses represent fermions in the presence of an external magnetic field.

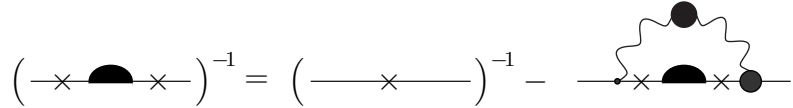


FIG. 2. The Schwinger-Dyson equation for the fermion self-energy. The curly line indicates the $U_S(1)$ statistical photon. Solid lines with crosses represent fermions in the presence of the external magnetic field. Blobs indicate quantum corrections (loops), which are ignored in the ladder approximation. Quantum dynamics of the electromagnetic field has been suppressed.

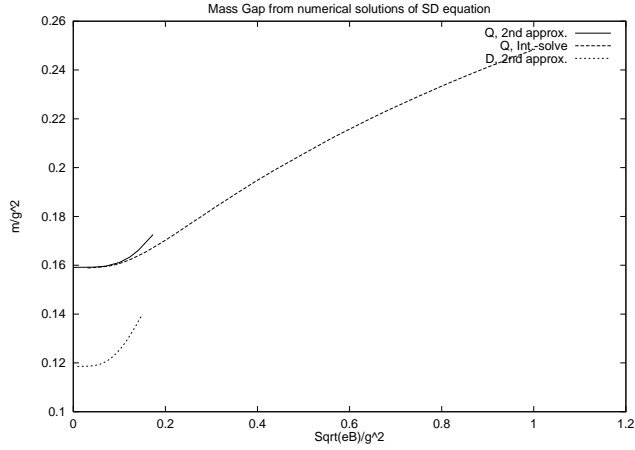


FIG. 3. Solution of Schwinger-Dyson equations for the quenched and dynamical fermions.

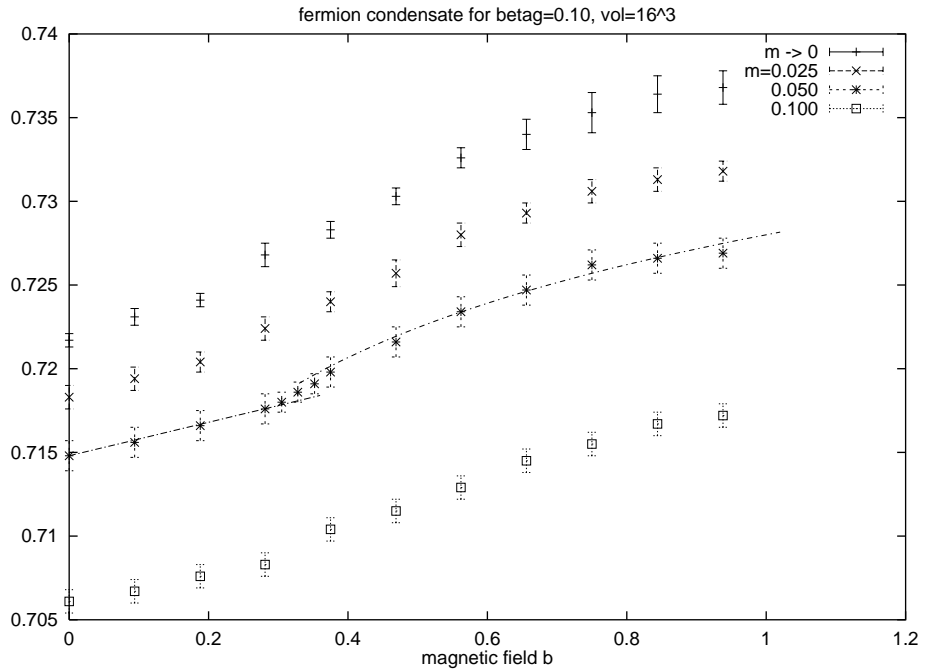


FIG. 4. $\langle \bar{\Psi} \Psi \rangle$ versus the magnetic field strength at strong coupling for three masses and extrapolation to the zero mass limit.

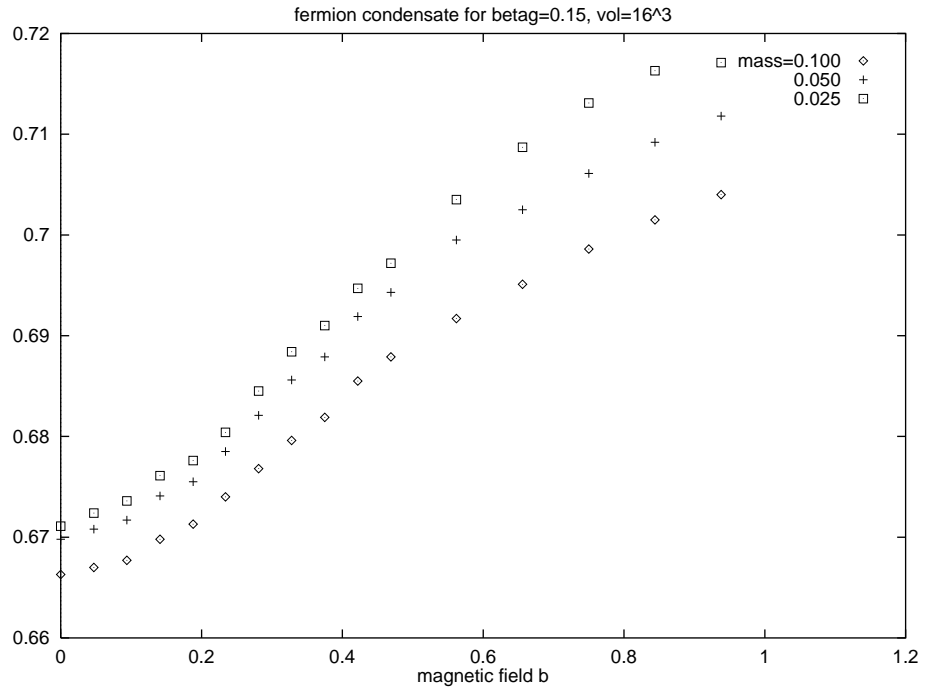


FIG. 5. $\langle \bar{\Psi} \Psi \rangle$ versus magnetic field strength at intermediate coupling for three masses.

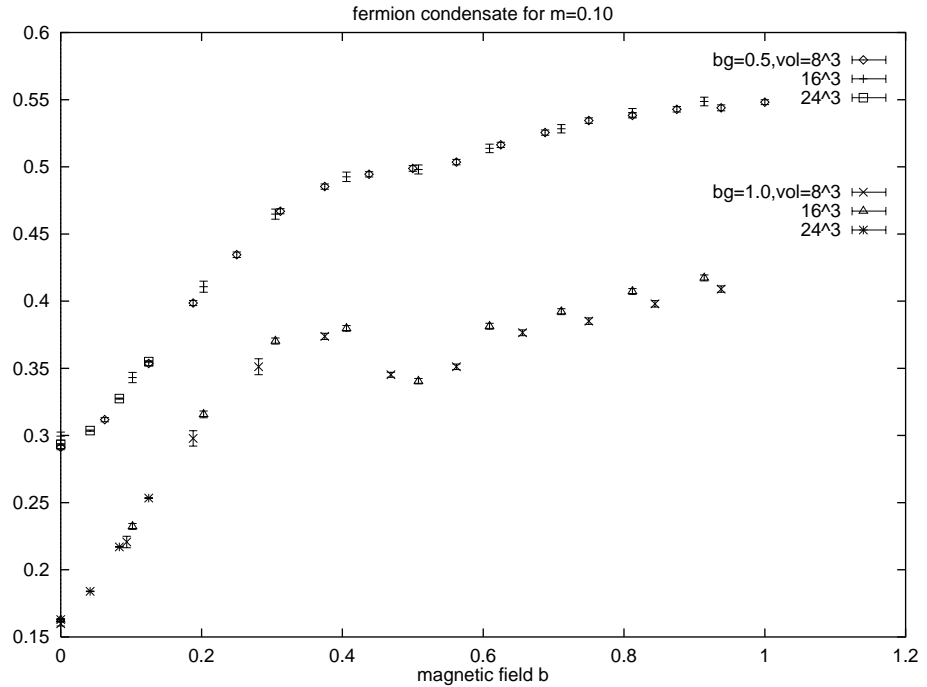


FIG. 6. $\langle \bar{\Psi} \Psi \rangle$ versus the magnetic field for two big values of the gauge coupling constant and three volumes.

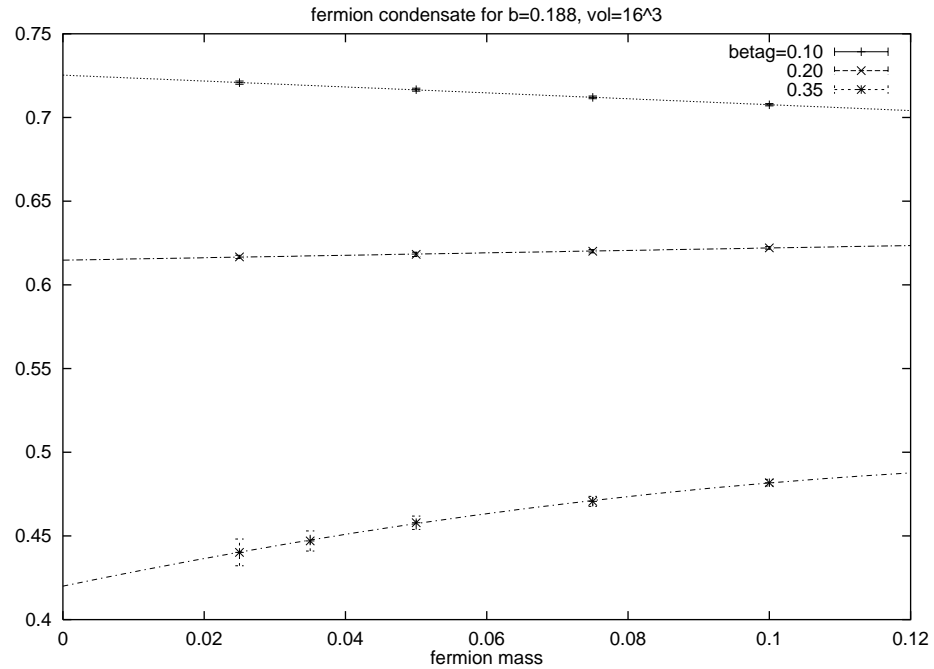


FIG. 7. $\langle \bar{\Psi} \Psi \rangle$ versus m for a typical value of the magnetic field strength and various values of β_G .

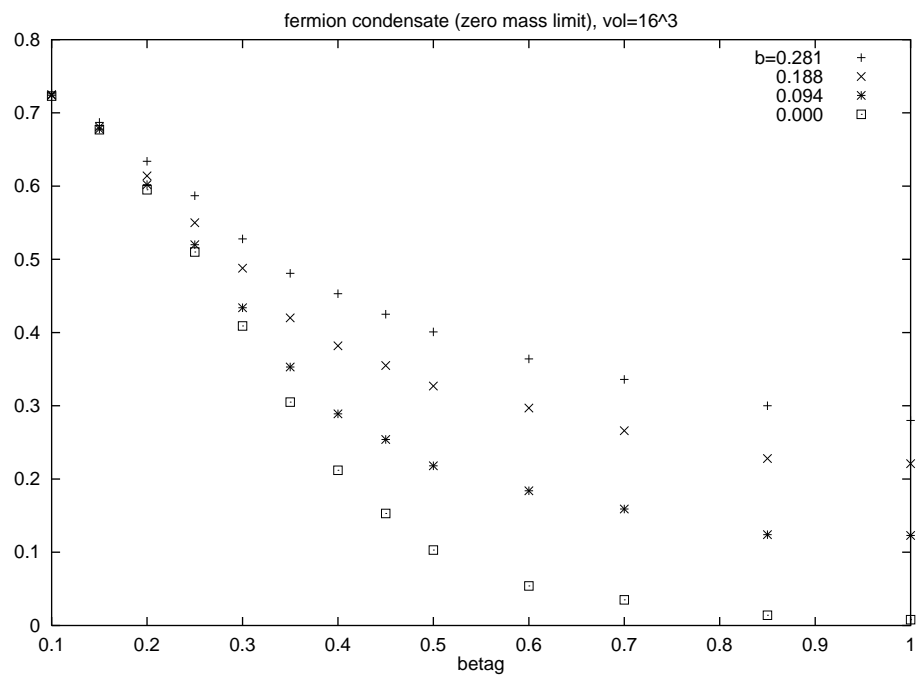


FIG. 8. $\langle \bar{\Psi} \Psi \rangle$ versus β_G in the zero mass limit for four values of the magnetic field strength.

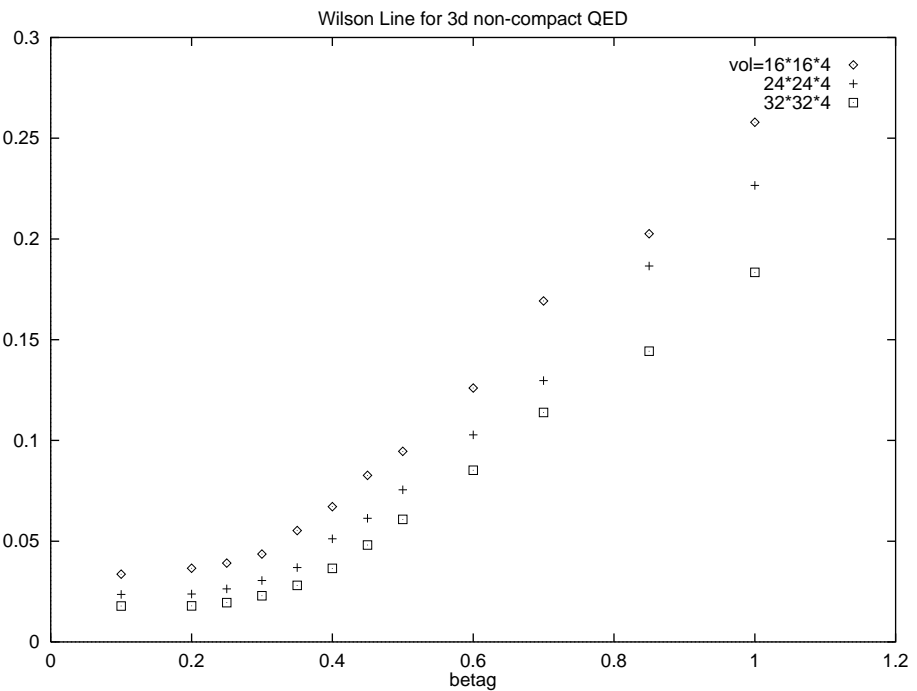


FIG. 9. Wilson line versus β_G for $N_\tau = 4$ and three spatial sizes.

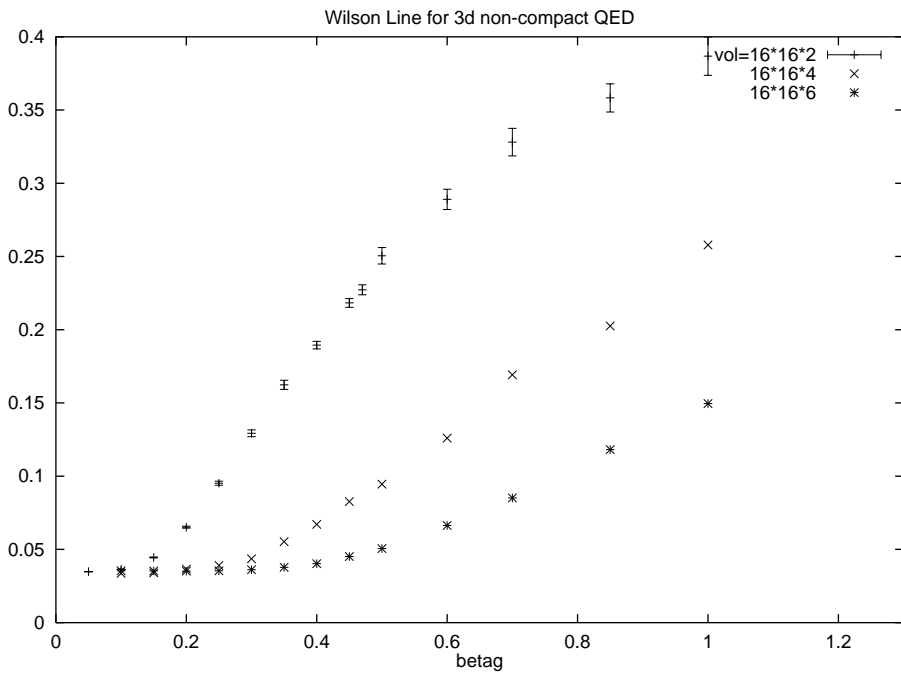


FIG. 10. Wilson line versus β_G for $N_\tau = 2$, $N_\tau = 4$ and $N_\tau = 6$.

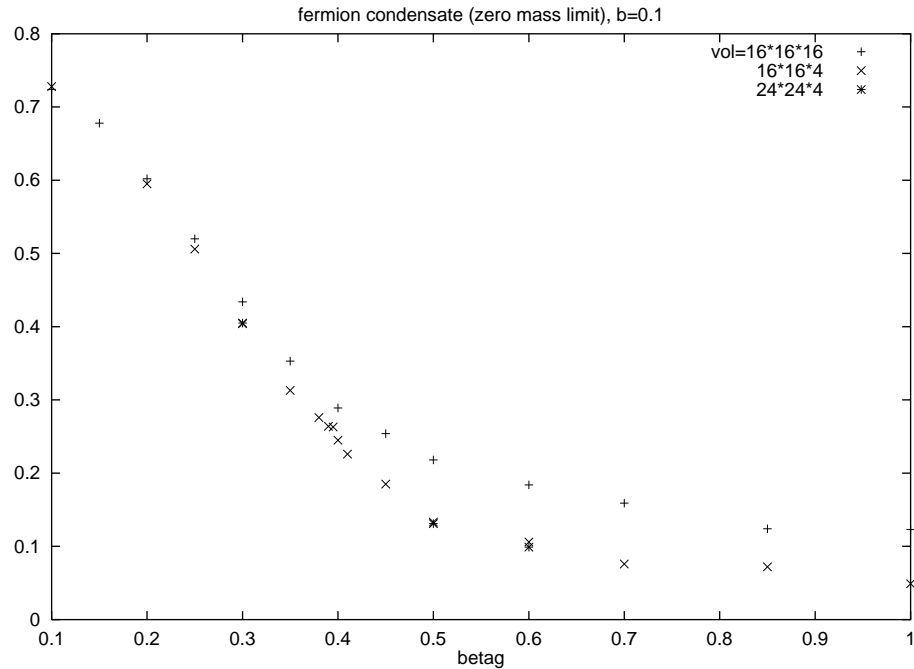


FIG. 11. Condensate versus β_G for $b=0.1$. Comparison of zero temperature with finite temperature.

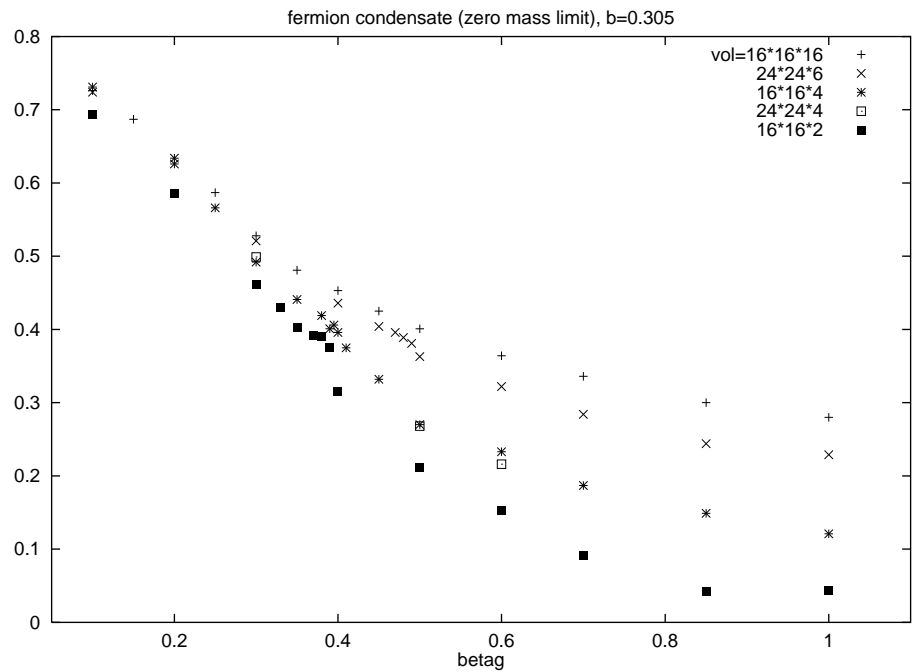


FIG. 12. Condensate versus β_G for $b=0.3$. Comparison of zero temperature with finite temperature. The error bars(not shown) are almost of the size of the symbols.

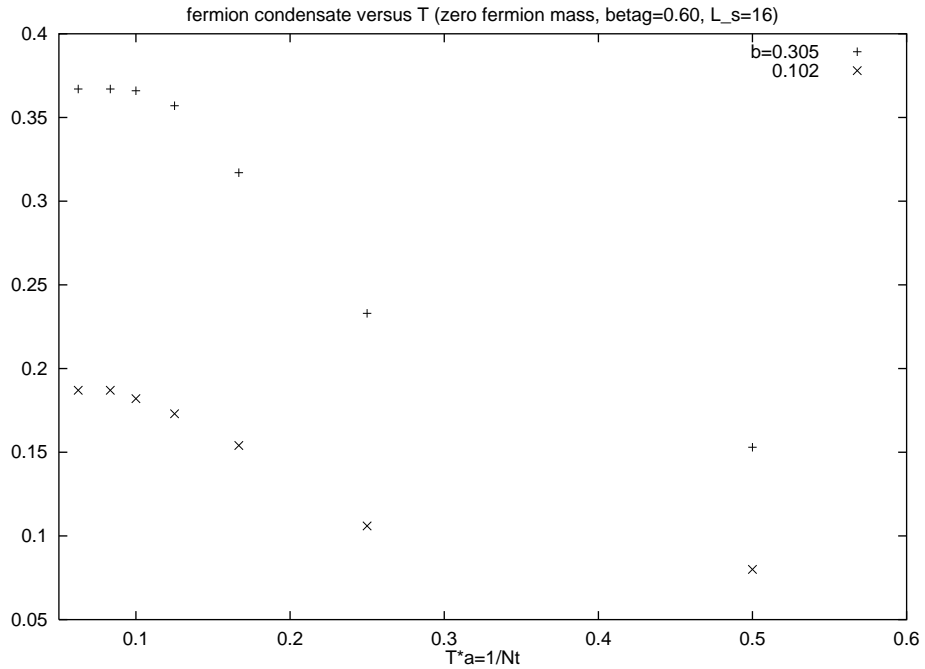


FIG. 13. $\langle \bar{\Psi} \Psi \rangle$ versus the temperature for two values of the magnetic field.

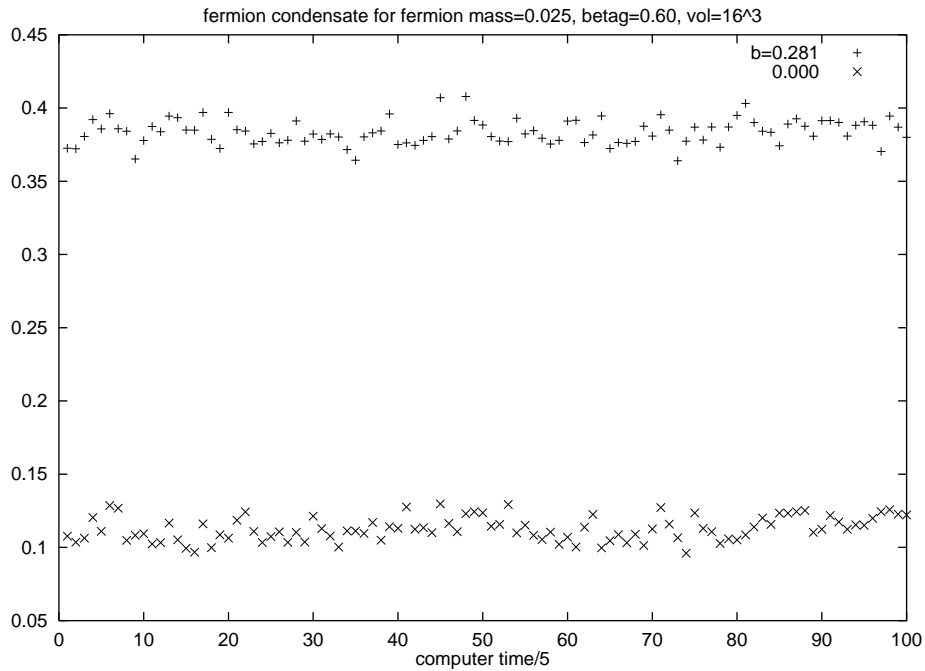


FIG. 14. Time evolution of $\langle \bar{\Psi} \Psi \rangle$ for a symmetric (16^3) lattice and two values of the magnetic field.

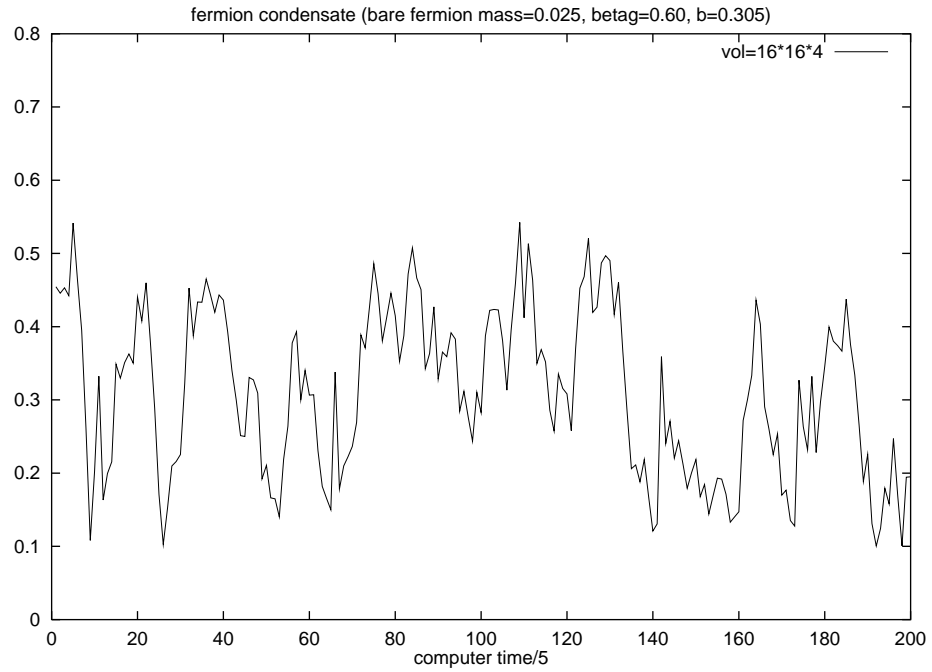


FIG. 15. Time evolution of $\langle \bar{\Psi} \Psi \rangle$ for a $16^2 * 4$ lattice.

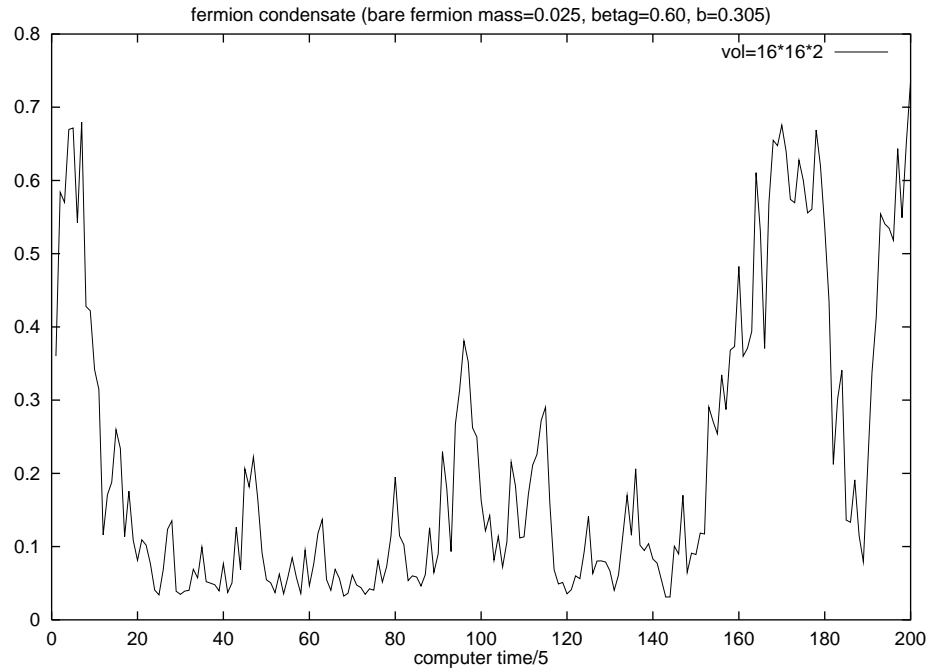


FIG. 16. Time evolution of $\langle \bar{\Psi} \Psi \rangle$ for a $16^2 * 2$ lattice.

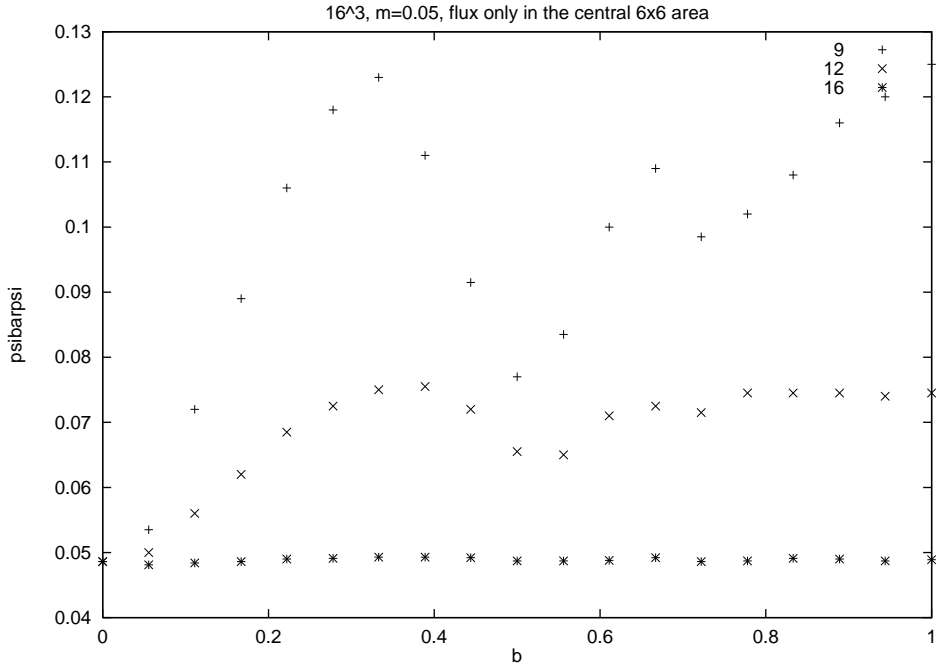


FIG. 17. $\langle \bar{\Psi} \Psi \rangle$ versus magnetic field strength where the flux is non zero only in a central region extending over 6×6 plaquettes. The condensate at sites labeled 9, 12, 16 (see text) is shown. The corresponding distances from the center of the flux tube are 0, 3, 7.

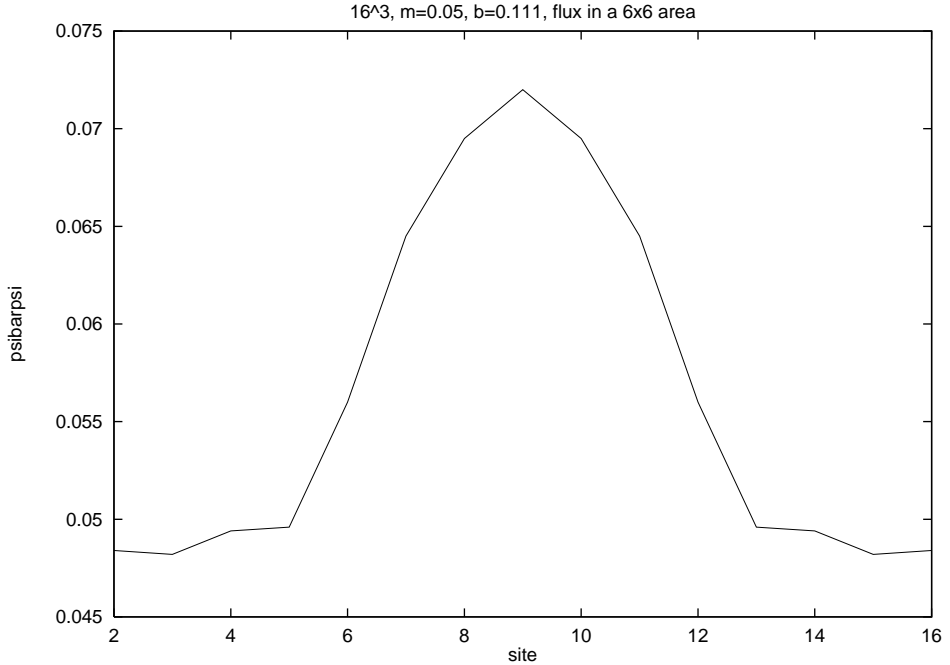


FIG. 18. $\langle \bar{\Psi} \Psi \rangle$ along a straight line passing from the center of the lattice if the magnetic field parameter b is set to 0.188. The central region of non-zero flux is 6×6 .